PNAS

Supporting Information for
Brain Representations of Affective Valence and Intensity in Sustained
Pleasure and Pain

Soo Ahn Lee, Jae-Joong Lee, Jisoo Han, Myunghwan Choi, Tor D. Wager, Choong-Wan Woo

Jae-Joong Lee & Choong-Wan Woo
Email: indaydream@skku.edu, waniwoo@skku.edu

This PDF file includes:

Supporting Information Text

Discussion

It is important to note that the insula anterior long gyrus, which included the dorsal posterior part of the insular cortex that is well-known for its involvement in pain processing (1), was not predictive of pain in our results (**Fig. 2**), even with using a more fine-grained insular parcellation or reducing sizes of the searchlight analyses (*SI Appendix*, **Fig. S28**). However, in our univariate voxel-wise analysis using TR-level data, the dorsal posterior insula appeared to track within-individual changes in ratings for pain (*SI Appendix*, **Fig. S29**). This is in line with a previous study (1) showing that the dorsal posterior insula encodes capsaicin-induced heat pain in the univariate analysis. The inconsistent results from the two analyses might be attributed to the fact that univariate analyses treat the between-individual variability as a random effect whereas our multivariate models were trained to capture the variability. While within-individual variability in pain and pleasure would be closely related to the levels of stimulus intensity or salience, between-individual variability may contain additional information about valence or evaluative processes. Therefore, we chose to capture both the within- and between-individual variability in predictive modeling. When we conducted region-level predictive modeling while minimizing the effect of between-individual variability, similar to the univariate analyses, the dorsal posterior insula was significantly predictive of pain (*SI Appendix*, **Fig. S30**). Thus, the absence of dorsal posterior insula in pain-predictive regions might be because the predictive model of this region did not explain the between-individual variability of pain, corresponding with previous studies that dorsal posterior insula is primarily involved in stimulus intensity coding than subjective evaluation of pain (2, 3).

The searchlight analysis results had a fewer number of overlapping voxels within the lateral prefrontal cortex (lPFC) regions that were part of the 7 overlapping brain regions (i.e., lPFC05, 09, and 14) compared to the ROI-based analysis results (**Fig. 2B**). However, with the same level of thresholding as in the ROI-based analysis (P < 0.0120), we were able to identify more overlapping voxels within the lPFC regions (**Fig. S11**). This suggests that these regions had relatively marginal significance in separately predicting pain or pleasure ratings compared to other overlapping brain regions. However, these regions appeared to be important for predicting intensity and valence scores (**Figs. 3D** and **4E**).

Note that the association between the explained variance and the decoding performance across 48 ROIs was negative, albeit not significant, for both pain and pleasure prediction (**Fig. S8A**). While the direction of this association in searchlight analysis was non-significant and inconsistent (**Fig. S10B**), we speculate that the negative association observed in ROI-level analysis may be due to the bias-variance tradeoff. That is, models based on PCs with larger explained variances may include more noises and thus lead to overfitting, which could reduce generalizability over the test datasets.

While we used the same fMRI experimental protocols, there were significant differences in the overall ratings of pain and pleasure intensity ratings between Studies 1 and 2 (**Fig. S3A**; capsaicin: $t(118)$ = 4.06, P = 8.94×10^{-5}, chocolate: $t(118)$ = 2.28, P = 0.0243, two-sample t-test, two-tailed). As a potential explanation for these differences, Study 2 included additional experimental conditions featuring diverse combinations of capsaicin and chocolate fluid deliveries within a run, whereas Study 1 only included the capsaicin- and chocolate-only conditions. Despite counterbalancing efforts, this may have influenced participants' overall perception of these fluids and led to an overall decrease in stimulus intensity ratings of these fluids. These differences between Studies 1 and 2 were even more pronounced in the chocolate condition than in the capsaicin condition. The overall level of ratings was reduced, and the changes were slower in Study 2 compared to Study 1 (**Table S5** and **Fig. S31**). The diminished quantity of chocolate fluid delivered to participants in Study 2 compared to Study 1 (Study 1 = 4.70±0.93 ml, Study 2 = 3.89±1.03 ml, $t(118)$ = 4.80, P = 4.68×10^{-6}) might further explain these differences. Despite efforts to maintain the fluid delivery system consistent across the two-year interval between studies, we cannot dismiss the possibility of unidentified variables influencing chocolate fluid deliveries.

Overall, these factors may have synergistically contributed to the observed differences between Studies 1 and 2.

Materials and Methods

Participants. In Study 1, fifty-eight healthy, right-handed participants were included (27 females, M_{age} = 22.81, SD_{age} = 2.83). We recruited participants from the Suwon area in the Republic of Korea. The preliminary eligibility of participants was determined through an online questionnaire, and those who had psychiatric, neurological, or systemic disorders and MRI contraindications were excluded. In Study 2, sixty-two healthy, right-handed participants were included (29 females, M_{age} = 22.69, SD_{age} = 2.66) based on the same recruitment criteria. Study 1 served as a 'training dataset' and was used for developing and evaluating predictive models. Study 2 was an 'independent test dataset' used only for the evaluation of the predictive models of intensity and valence.

Experimental design. The fMRI experiment in Studies 1 and 2 consisted of three conditions; (1) 'control,' (2) 'capsaicin' (i.e., pain), and (3) 'chocolate' (i.e., pleasure) conditions. The orders of these three conditions were counterbalanced across participants. To deliver liquids to participants, we used the custom-built 8-channel fluid delivery system (Octaflow II, ALA Scientific Instruments Inc., Westbury, NY) and a custom-built MR-compatible mouthpiece, where plastic tubes were inserted and connected to Tygon tubes to deliver and extract fluids. In addition, we used a suction device (Join Medical, Inc.) to remove fluids from a participant's oral cavity during the experiment. The use of this suction procedure helped to minimize head movements caused by the swallowing of fluids.

      For the 'control' condition, we delivered only water at a very slow speed (about 1.25 ml/min) while participants were relaxed and instructed to continuously rate their current state of pleasantness and unpleasantness using an MR-compatible trackball device. For the 'capsaicin' and 'chocolate' conditions, capsaicin or chocolate fluids were delivered twice during each scan—first after 90 seconds and then after 7 minutes from the beginning of the scan. Water was delivered at all other times. During scans, we asked participants to rate their subjective level of pleasantness or unpleasantness continuously.

      For the capsaicin fluid, we used capsaicin-rich hot sauce (Jinmifood, Inc.), which was diluted with water to a concentration of around 20% (v/v). The capsaicin fluid was delivered for a duration of 90 seconds each, with a delivery volume of 0.28±0.11 ml [mean±SD] for each delivery in Study 1, and 0.31±0.11 ml for each delivery in Study 2. For the chocolate fluid, we used hot chocolate powder (Hershey's, Inc.), which was dissolved in water to a concentration of around 30% (w/v). The chocolate fluid was delivered for a duration of 3 minutes each, with a delivery volume of 4.70±0.93 ml for each delivery in Study 1, and 3.89±1.03 ml for each delivery in Study 2. For more discussion of this experimental difference, please see *SI Appendix*, **Supplementary discussion**. The duration of fluid delivery was different between capsaicin and chocolate to match the duration of induced pleasure and pain experience similar between the two conditions. To minimize the residual effects of the capsaicin and chocolate fluids, we washed out participants' oral cavity with water after each condition until they reported no lingering taste. In addition, we conducted the structural scan after the capsaicin condition to allow sufficient time for any remaining painful sensation to be alleviated.

Rating scale. We used a modified version of the general Labeled Magnitude Scale (gLMS) for the pleasantness-unpleasantness rating. The scale was bidirectional with the center of the scale indicating "Not at all" (0) and the extremes of both sides indicating "Strongest imaginable unpleasantness of any kind" (-1) and "Strongest imaginable pleasantness of any kind" (1). The anchors were "Weak" (0.061), "Moderate" (0.172), "Strong" (0.354), and "Very strong" (0.533) on both sides. Before the fMRI scans, we provided a detailed explanation of how to use the rating scale while showing the anchors, but the anchors were not shown on the screen during the scan. To reduce the potential confounding effects of rating directionality, we randomly switched the labels of two rating extremes (i.e., pleasantness and unpleasantness) across participants.
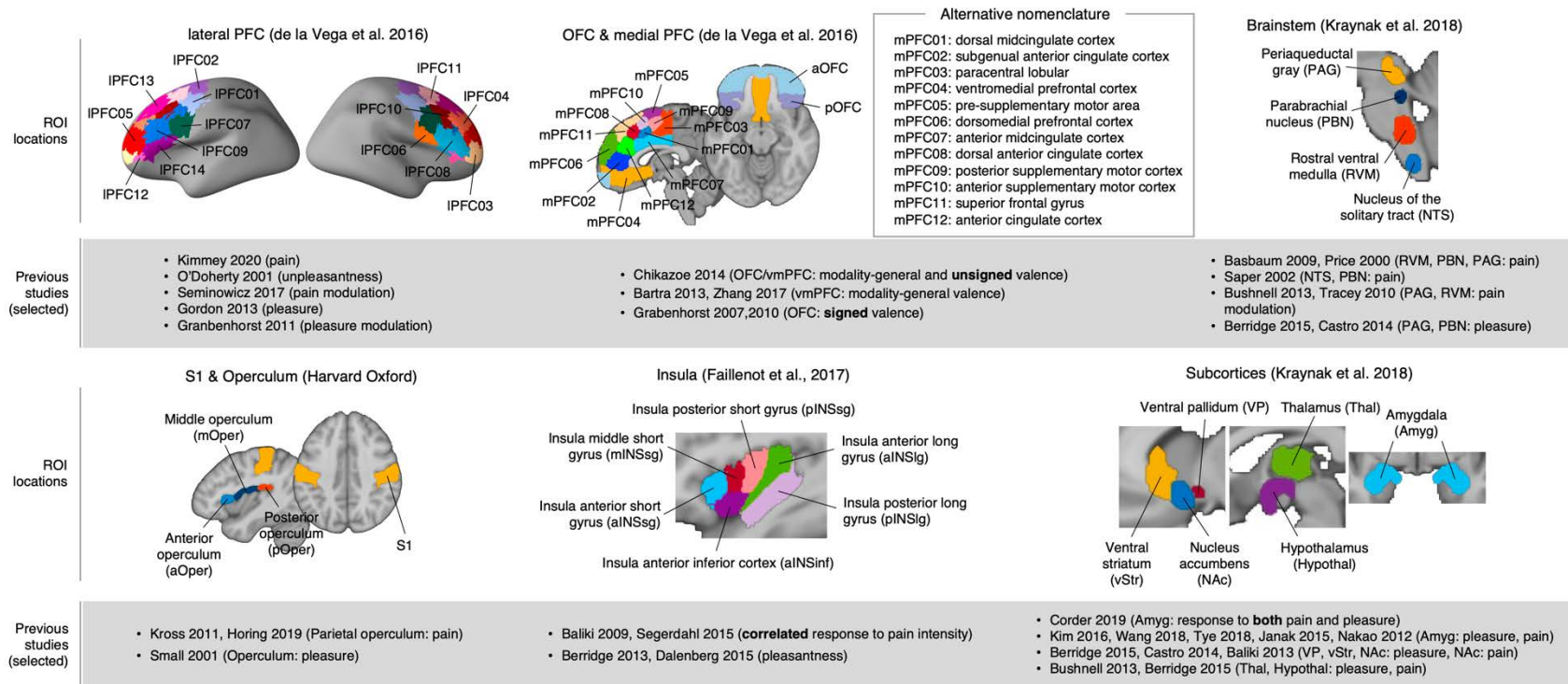
fMRI data acquisition. Whole-brain fMRI data were acquired on a 3T Siemens Prisma scanner in the Center for Neuroscience Imaging Research at Sungkyunkwan University. High-resolution T1-weighted structural images were acquired. Functional EPI images were acquired with TR = 460 ms, TE = 27.2 ms, multiband acceleration factor = 8, field of view = 220 mm, 82 × 82 matrix, 2.7 × 2.7 × 2.7 mm^3 voxels, 56 interleaved slices, number of volumes = 1893. We used Matlab (Mathworks) and Psychtoolbox (http://psychtoolbox.org/) for the stimulus presentation and behavioral data acquisition.

fMRI data analysis. Structural and functional MRI data were preprocessed using our in-house preprocessing pipeline (https://github.com/cocoanlab/humanfmri_preproc_bids). This pipeline utilizes preprocessing tools in FSL and SPM12. We removed 18 initial volumes of functional EPI images for image intensity stabilization. Then, we co-registered structural T1-weighted images to the functional images and normalized them to MNI, and the functional EPI images were distortion-corrected, motion-corrected (realigned), normalized to MNI using T1 images with the interpolation to 2 × 2 × 2 mm^3 voxels, and smoothed with a 5-mm FWHM Gaussian kernel. We then used 25-second time bin regressors convolved with the hemodynamic response function for GLM analysis and obtained 34 beta images. In the GLM analysis, we included nuisance covariates including 24 head motion parameters (x, y, z, roll, pitch, and yaw, their mean-centered squares, their derivatives, and squared derivative), linear drift, outlier indicators, and five principal components of white matter signals and those of ventricle signals. We also winsorized the values that were detected as spatiotemporal outliers (intensity values < median minus 5 SDs or > median plus 5 SDs) and applied a low pass filter with a 0.1 Hz threshold. The resulting beta images were concatenated and rescaled across participants and conditions in the SPM style (i.e., L1 normalization). We used these data as input features for the predictive modeling. We also down-sampled the pleasantness-unpleasantness ratings into 34 time-bins and used them as an outcome variable for the predictive modeling. A graphical illustration of making 34-bin data of fMRI and behavioral data is shown in ***SI Appendix,* Fig. S4A**.

Choosing the number of principal components for region-level information mapping. Since the choice of the number of principal components (PCs) affects the number of free parameters of the model and thus has a significant impact on model performance, particularly in terms of its generalizability (e.g., in cross-validation), we used the same number of PCs for all 48 regions to strike a balance between capturing sufficient variance in the data and avoiding excessive complexity. To determine the number of PCs a priori, we first averaged all the time-bin data for each condition and concatenated the averaged fMRI data across the 'capsaicin' and 'control' conditions or across the 'chocolate' and 'control' conditions, obtaining two images per participant, resulting in a total of 116 images (= 2 images × 58 participants) for each condition. Then, we applied principal component analysis (PCA) to the concatenated data to find the minimum required number of components to explain > 75% of the total variance. We repeated this procedure for each ROI, obtained a total of 96 different PC numbers (= 48 ROIs × 2 conditions), and selected the median of the PC numbers, which was 13 PCs (graphical illustration is provided in ***SI Appendix***, **Fig. S4B** and **4C**).

Searchlight analysis. To examine the robustness of the region-level information mapping results, we repeated the predictive modeling with searchlights. For this, we created a searchlight with a radius of five voxels and scanned it throughout the whole brain with a step size of four voxels. The number of PCs was the same with the region-level predictive modeling (= 13) for consistency. We developed a PCR model for each searchlight region, evaluated the prediction performance with LOSO-CV, and added this value to cubes that had one side of four voxels and were located at the center of each searchlight across the whole brain with no overlapping voxels between cubes. We smoothed the performance maps of pain and pleasure models with a 3-mm FWHM Gaussian kernel, and thresholded results based on the bootstrap test with 10,000 iterations and FDR correction. We conducted the additional searchlight analysis (***SI Appendix***, **Fig. S28B**) based on the same procedure, but using a searchlight with a radius of three voxels.

Rank-based subsampling. In developing the intensity and valence models, there was an issue in using the concatenated ratings across different conditions—the rating magnitudes for the capsaicin condition were greater than those for the chocolate condition, creating a skewness of the data distribution and thus introducing a potential bias in the modeling. To minimize the potential bias, we subsampled the data with a stratified sampling method to match the numbers of positive (i.e., pleasantness) and negative (i.e., unpleasantness) rating data. In more detail, we first split the rating data into ten equidistant bins and transformed them into positive and negative ranks (i.e., 1, 2, …, 10 and -1, -2, …, -10), except for zeros. We then compared the frequency of positive and negative values in a bin-by-bin manner, i.e., the number of data points within the bin +1 vs. -1, +2 vs. -2, ..., and matched the frequency by random subsampling of data from the bin that had more data. Consequently, the distributions of the positive and negative values became symmetric. We developed the intensity and valence models using these subsampled data.

lateral PFC (de la Vega et al. 2016)

lPFC02
lPFC13
lPFC01
lPFC05
lPFC07
lPFC09
lPFC14
lPFC12

lPFC11
lPFC04
lPFC10
lPFC06
lPFC08
lPFC03

OFC & medial PFC (de la Vega et al. 2016)

mPFC05
mPFC10
mPFC08
mPFC09
mPFC03
mPFC11
mPFC01
mPFC06
mPFC07
mPFC02
mPFC12
mPFC04

aOFC
pOFC

Alternative nomenclature

mPFC01: dorsal midcingulate cortex
mPFC02: subgenual anterior cingulate cortex
mPFC03: paracentral lobular
mPFC04: ventromedial prefrontal cortex
mPFC05: pre-supplementary motor area
mPFC06: dorsomedial prefrontal cortex
mPFC07: anterior midcingulate cortex
mPFC08: dorsal anterior cingulate cortex
mPFC09: posterior supplementary motor cortex
mPFC10: anterior supplementary motor cortex
mPFC11: superior frontal gyrus
mPFC12: anterior cingulate cortex

Brainstem (Kraynak et al. 2018)

Periaqueductal gray (PAG)
Parabrachial nucleus (PBN)
Rostral ventral medulla (RVM)
Nucleus of the solitary tract (NTS)

ROI locations

Previous studies (selected)

- Kimmey 2020 (pain)
- O'Doherty 2001 (unpleasantness)
- Seminowicz 2017 (pain modulation)
- Gordon 2013 (pleasure)
- Granbenhorst 2011 (pleasure modulation)

- Chikazoe 2014 (OFC/vmPFC: modality-general and **unsigned** valence)
- Bartra 2013, Zhang 2017 (vmPFC: modality-general valence)
- Grabenhorst 2007,2010 (OFC: **signed** valence)

- Basbaum 2009, Price 2000 (RVM, PBN, PAG: pain)
- Saper 2002 (NTS, PBN: pain)
- Bushnell 2013, Tracey 2010 (PAG, RVM: pain modulation)
- Berridge 2015, Castro 2014 (PAG, PBN: pleasure)

S1 & Operculum (Harvard Oxford)

Middle operculum (mOper)
Posterior operculum (pOper)
Anterior operculum (aOper)
S1

Insula (Faillenot et al., 2017)

Insula posterior short gyrus (pINSsg)
Insula middle short gyrus (mINSsg)
Insula anterior long gyrus (aINSlg)
Insula anterior short gyrus (aINSsg)
Insula posterior long gyrus (pINSlg)
Insula anterior inferior cortex (aINSinf)

Subcortices (Kraynak et al. 2018)

Ventral pallidum (VP)
Thalamus (Thal)
Amygdala (Amyg)
Ventral striatum (vStr)
Nucleus accumbens (NAc)
Hypothalamus (Hypothal)

ROI locations

Previous studies (selected)

- Kross 2011, Horing 2019 (Parietal operculum: pain)
- Small 2001 (Operculum: pleasure)

- Baliki 2009, Segerdahl 2015 (**correlated** response to pain intensity)
- Berridge 2013, Dalenberg 2015 (pleasantness)

- Corder 2019 (Amyg: response to **both** pain and pleasure)
- Kim 2016, Wang 2018, Tye 2018, Janak 2015, Nakao 2012 (Amyg: pleasure, pain)
- Berridge 2015, Castro 2014, Baliki 2013 (VP, vStr, NAc: pleasure, NAc: pain)
- Bushnell 2013, Berridge 2015 (Thal, Hypothal: pleasure, pain)

Fig. S1. 48 *a priori* regions-of-interest (ROIs) (related to Figs. 1-2). We selected the 48 brain regions *a priori* that have been reported to be responsive to either pain or pleasure. First, the lateral prefrontal cortex has been known to be related to pain, pleasure, and their modulation (5-9). Second, the orbitofrontal and medial prefrontal cortices have been heavily studied in terms of their modality-general valence processing (10-14). We also provided the alternative nomenclature of the medial prefrontal regions based on their anatomy. Third, the primary somatosensory cortex (S1) and operculum have been reported as pain and pleasure-responsive regions (15-17). Fourth, the brainstem regions including the nucleus of the solitary tract, rostral ventral medulla, parabrachial nucleus, and periaqueductal gray, are known to be part of ascending and descending pain pathways as well as of pleasure pathways (18-24). Fifth, the insular cortex has been known to encode pleasantness (25, 26), and particularly, the dorsal posterior insula (especially near the parietal operculum) has shown to be correlated with pain intensity (1, 27). Sixth, the ventral striatum, nucleus accumbens, ventral pallium, thalamus and hypothalamus are also known to be important for processing pain and

pleasure (21, 23, 24, 28). Lastly, the amygdala has been heavily studied due to its response both to pain and pleasure (29-34). We used the defined ROIs from previous studies, for brainstem and subcortical regions, ref. (35), for insular regions, ref. (36), and for lateral and medial prefrontal cortices (PFC), ref. (37). We used the Harvard-Oxford brain atlas for S1 and opercular regions.
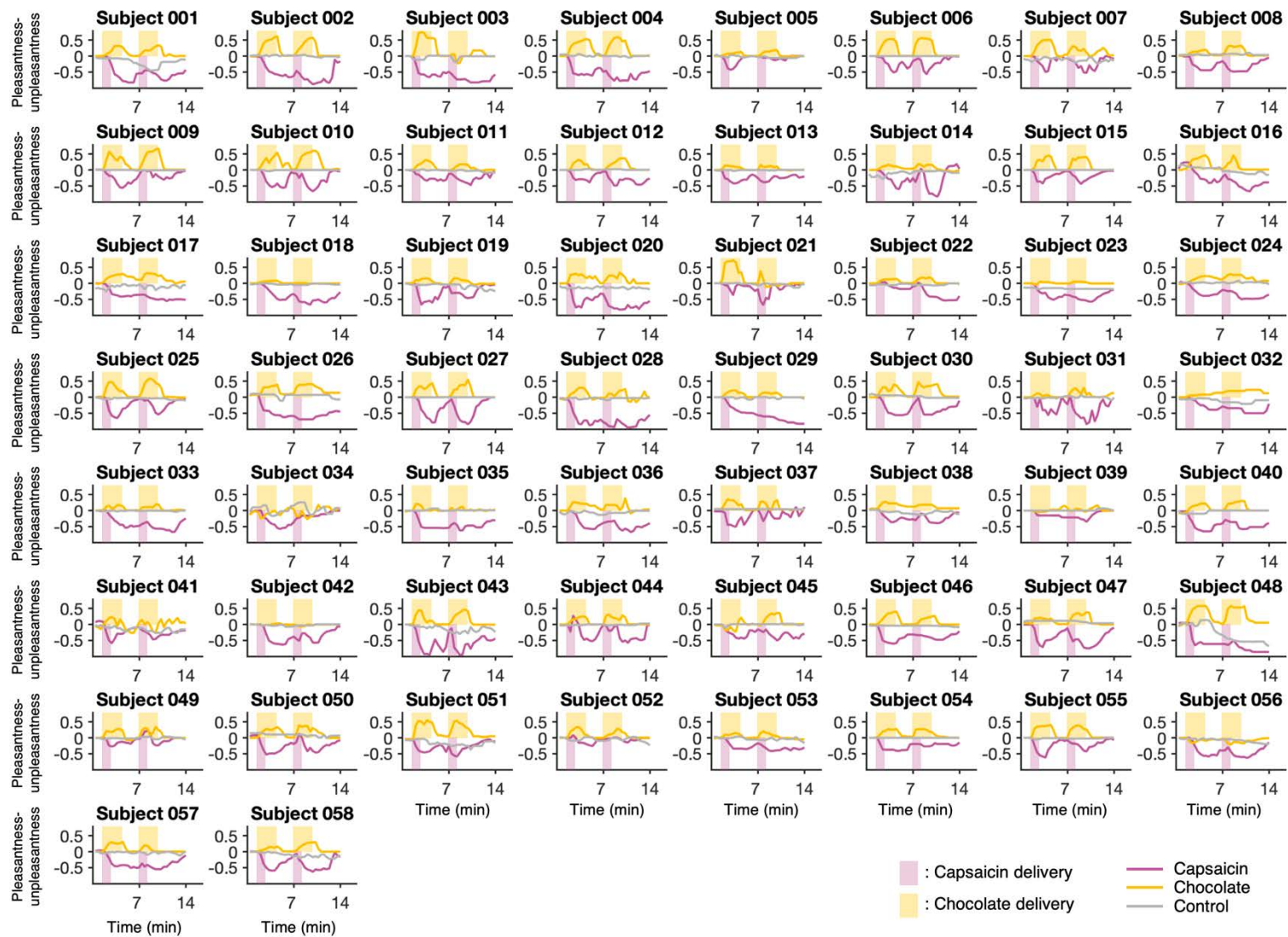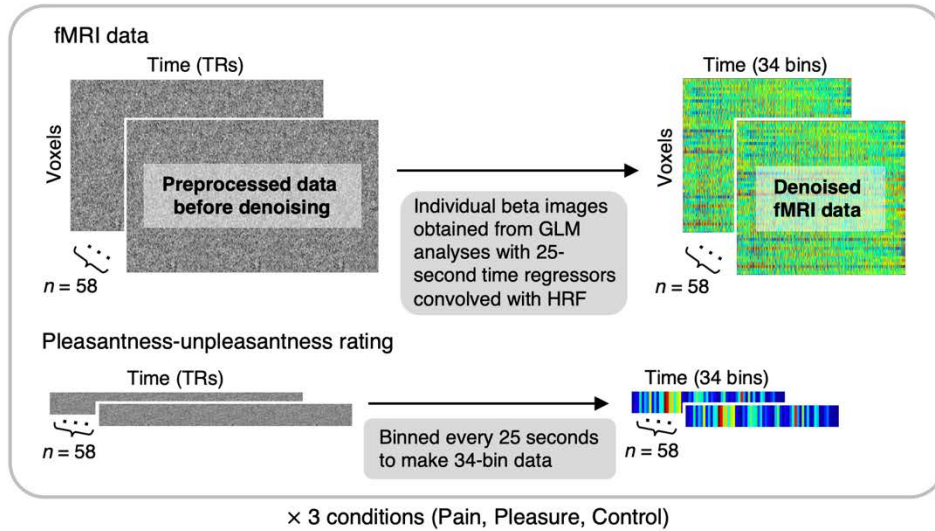
Fig. S2. Individual rating trajectories of the capsaicin, chocolate, and control conditions (*N* = 58; related to Fig. 1). Individual rating trajectories of 58 participants from Study 1. 55 out of 58 participants (94.8%) reported their maximum pain levels exceeding 'strong' (0.354) on the gLMS scale in the capsaicin condition, while 25 participants (43.1%) reported their maximum pleasure levels over strong (0.354), and 51 participants (87.9%) reported their maximum pleasure levels over moderate (0.172) in the chocolate conditions. The purple, yellow, and grey solid lines show the pleasantness-unpleasantness ratings for the capsaicin, chocolate, and control conditions, respectively. Transparent squares indicate the durations that each type of stimulus was administrated (1.5 minutes for capsaicin and 3 minutes for chocolate).
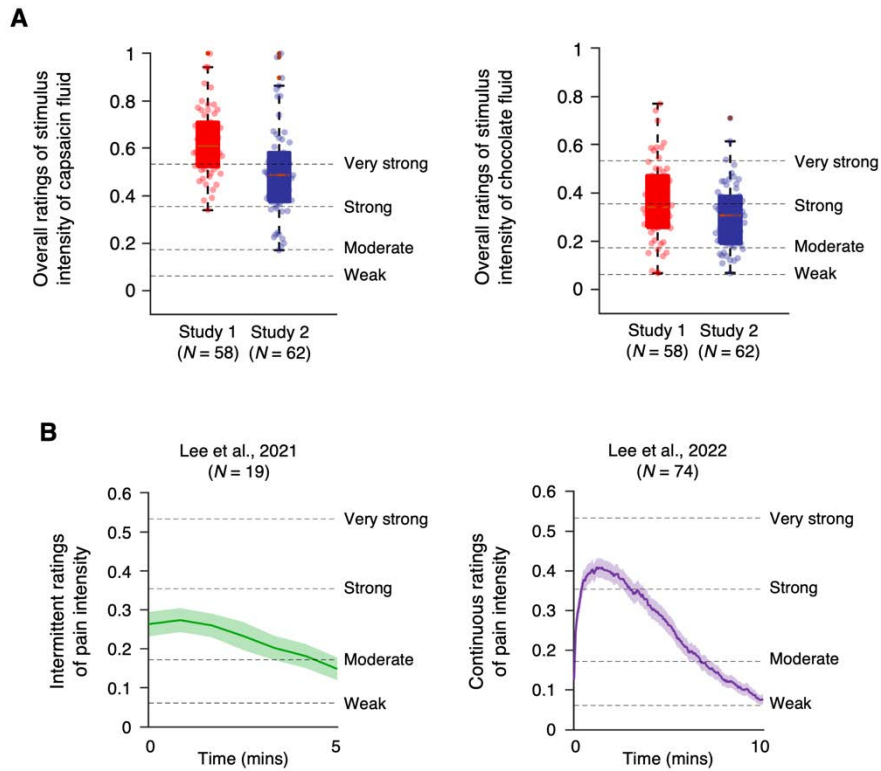
Fig. S3. Stimulus intensity ratings after and during capsaicin stimulation. (A) Overall intensity ratings for capsaicin and chocolate fluids obtained after the capsaicin and chocolate runs for Study 1 (*N* = 58, red) and Study 2 (*N* = 62, blue). The horizontal dashed lines indicate the anchors of the general labeled magnitude scale (gLMS (38)) modified for pain intensity ratings. **(B)** Left: Intermittent ratings of pain intensity for every 45 seconds from a previous study (Study 1 from ref. (39), *N* = 19, green). Right: Continuous ratings of pain intensity from a previous study (Study 2 from ref. (40), *N* = 74, purple).

A 34-bin beta images and pleasantness-unpleasantness ratings per each condition

fMRI data

Time (TRs)

Voxels

Preprocessed data before denoising

n = 58

Individual beta images obtained from GLM analyses with 25-second time regressors convolved with HRF

Time (34 bins)

Voxels

Denoised fMRI data

n = 58

Pleasantness-unpleasantness rating

Time (TRs)

n = 58

Binned every 25 seconds to make 34-bin data

Time (34 bins)

n = 58

× 3 conditions (Pain, Pleasure, Control)

B Selecting the number of PCs for dimension reduction

Pain & Control concatenated

Voxels

ROI

→ PCA →

Components

Averaged across bins, 58 participants

Obtain the reduced number of components explaining 75% of variance of concatenated ROI data

Pleasure & Control concatenated

Voxels

ROI

→ PCA →

Components

× 48 ROIs
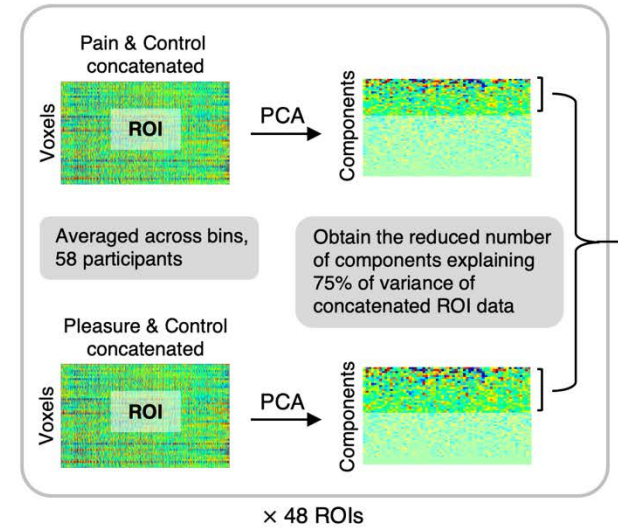
C Training PCR models with the selected number of PCs

Pain & Control or Pleasure & Control

Voxels

ROI

→ PCA →

Observations

Predictor: 13 PCs

• 34 bin x 58 participants
• Leave-one-out cross-validation

↓ Regression

Outcome: ratings

Select the median values of 2×48 number of components (which was 13 components)

X 48 ROIs

• Bootstrap using within-individual prediction performance
• FDR correction to find out significant ROIs
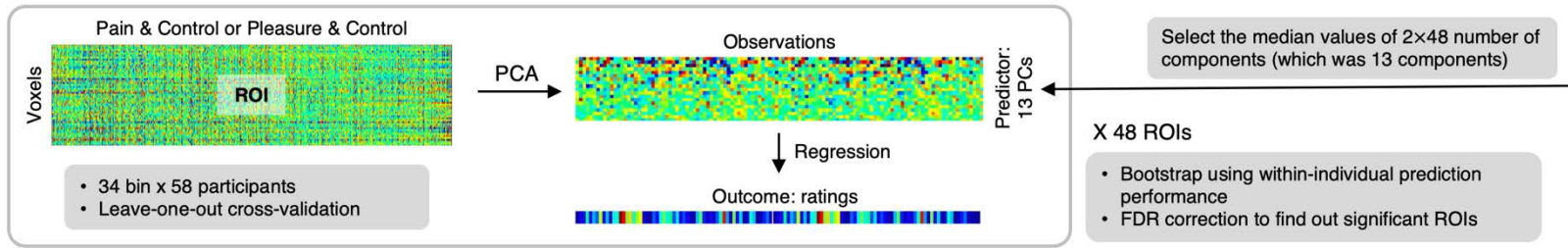
Fig. S4. Analysis overview of region-level predictive modeling (related to Fig. 2). (A) For the predictive modeling, we used 34-bin beta images of fMRI data as inputs. To obtain 34-bin beta images, we conducted general linear modeling (GLM) analyses with

25-second time-bin regressors convolved with the hemodynamic response function. We also included nuisance covariates (24 head motion parameters, linear drift, outlier indicators, and five principal components of white matter and ventricle signals) in the GLM analyses. We also averaged the pleasantness-unpleasantness ratings into 34 time-bins. **(B)** Given that the choice of the number of principal components (PCs) can influence the model training, we aimed to use the same number of PCs for all 48 regions. To determine the number of PCs, we first averaged all the time-bin data for each condition and concatenated the averaged fMRI data across the capsaicin and control conditions or across the chocolate and control conditions, obtaining two images per participant, resulting in a total of 116 images (= 2 images × 58 participants) for each condition. Then, we applied principal component analysis (PCA) to the concatenated data to find the minimum required number of components to explain > 75% of the total variance. We repeated this procedure for each ROI, obtained 96 different PC numbers (= 48 ROIs × 2 conditions), and selected the median of the PC numbers, which was 13 components. **(C)** Using this number of PCs, we applied the principal component regression (PCR) for each ROI to predict ratings for either the capsaicin and control conditions or the chocolate and control conditions, based on concatenated fMRI data across all the time-bins, conditions, and participants (i.e., 34 bins × 2 runs × 58 participants). We evaluated the mean within-individual correlation between predicted and actual outcomes with the leave-one-subject-out cross-validation and examined their statistical significance using bootstrap tests with 10,000 iterations. We used the false discovery rate (FDR) $q < 0.05$ to correct for the multiple comparisons.
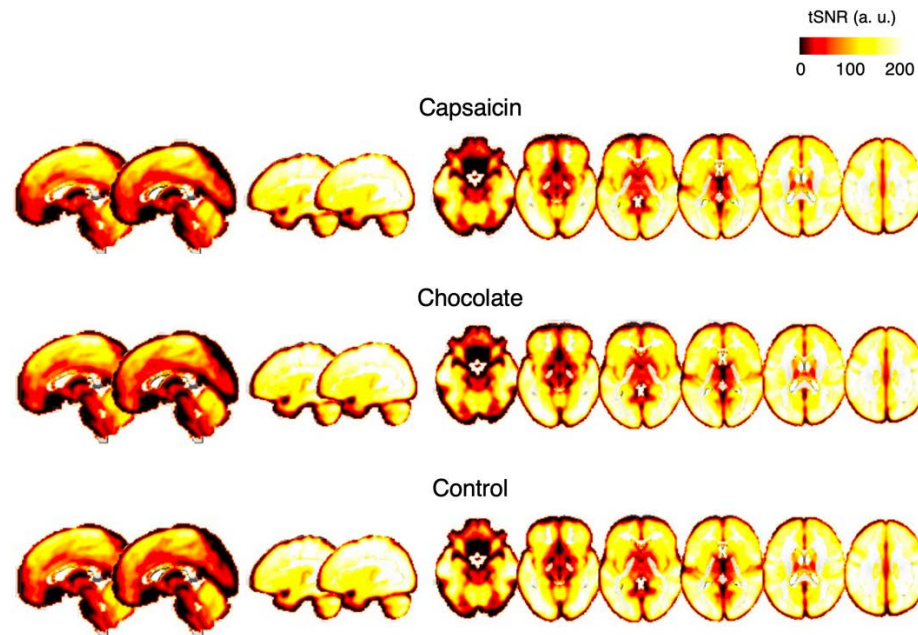
Fig. S5. Temporal Signal-to-Noise Ratio (tSNR) maps across capsaicin, chocolate, and control conditions in Study 1.
We calculated group-level temporal signal-to-noise ratio (tSNR) by calculating the ratio of the mean and standard deviation of voxel-wise fMRI timeseries for each condition and then averaging the resulting individual-level tSNR maps across participants. Note that the tSNR of the brainstem regions was lower compared to the other brain regions.
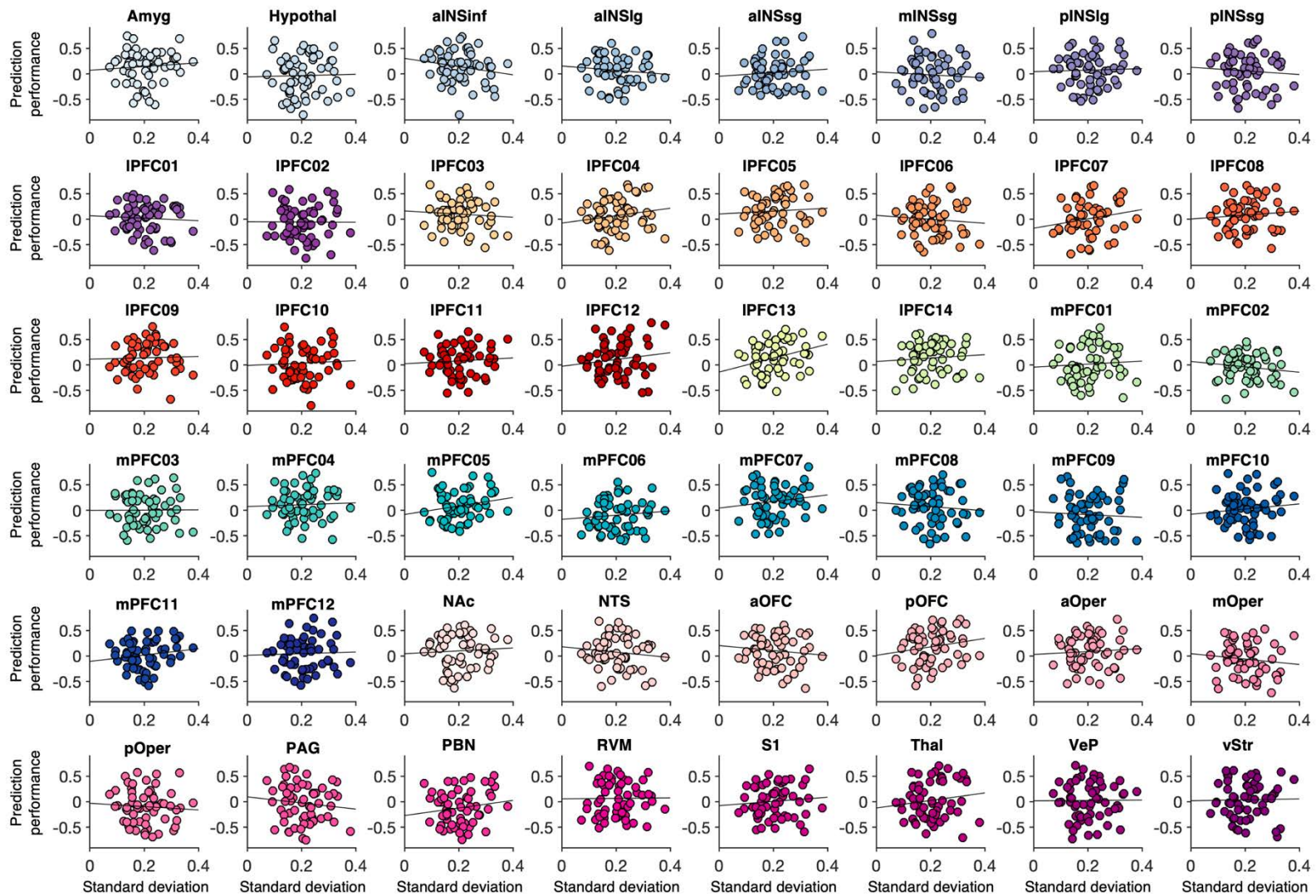
Fig. S6. Relationships between the region-level prediction performance of pain prediction models and standard deviation of ratings (related to Fig. 2). The plots show the relationship between the within-individual prediction-outcome

correlation of region-level pain prediction models and the standard deviation of the pleasantness-unpleasantness ratings across the capsaicin and control conditions. Dots and dot colors represent each individual and different ROIs, respectively. We found no significant correlations between the prediction performance and the standard deviation of the ratings (r = -0.18-0.31, all qs > 0.05, FDR corrected, one-sample t-test, two-tailed). Amyg: amygdala, Hypothal: hypothalamus, aINSinf: insula anterior inferior, aINSsg: insula anterior short gyrus, mINSsg: insula middle short gyrus, pINSlg: insula posterior long gyrus, pINSsg: insula posterior short gyrus, lPFC: lateral prefrontal cortex, mPFC: medial prefrontal cortex, NAc: nucleus accumbens, NTS: nucleus of the solitary tract, aOFC: anterior orbitofrontal cortex, pOFC: posterior orbitofrontal cortex, aOper: anterior operculum, mOper: middle operculum, pOper: posterior operculum, PAG: periaqueductal gray, PBN: parabrachial nucleus, RVM: rostral ventral medulla, S1: primary somatosensory cortex, Thal: thalamus, VeP: ventral pallidum, vStr: ventral striatum.

Fig. S7. Relationships between the region-level performances of pleasure prediction models and standard deviation of ratings (related to Fig. 2). Same as **Fig. S6**, but the relationship between the within-individual prediction-outcome correlation of region-level pleasure prediction models and the standard deviation of the pleasantness-unpleasantness ratings.

16

Again, we found no significant correlations between the prediction performance and the standard deviation of the ratings (r = -0.18-0.35, all qs > 0.05, FDR corrected, one-sample t-test, two-tailed). Amyg: amygdala, Hypothal: hypothalamus, aINSinf: insula anterior inferior, aINSsg: insula anterior short gyrus, mINSsg: insula middle short gyrus, pINSlg: insula posterior long gyrus, pINSsg: insula posterior short gyrus, lPFC: lateral prefrontal cortex, mPFC: medial prefrontal cortex, NAc: nucleus accumbens, NTS: nucleus of the solitary tract, aOFC: anterior orbitofrontal cortex, pOFC: posterior orbitofrontal cortex, aOper: anterior operculum, mOper: middle operculum, pOper: posterior operculum, PAG: periaqueductal gray, PBN: parabrachial nucleus, RVM: rostral ventral medulla, S1: primary somatosensory cortex, Thal: thalamus, VeP: ventral pallidum, vStr: ventral striatum.

Fig. S8. Relationship between the explained variance, region sizes, and the prediction performance across 48 ROIs. (related to Fig. 2A) Purple: pain prediction, yellow: pleasure prediction. **(A)** The relationship between the region-wise explained variance of 13 Principal Components (PCs) and the prediction performance. We found negative correlations with medium effect sizes between them (r = -0.27, P = 0.0647 for the pain prediction, and r = -0.26, P = 0.0780 for the pleasure prediction). However, they were not significant, possibly due to the small number of regions (n_{ROI} = 48), and thus caution should be used in interpreting these results. **(B)** The relationship between the region sizes and the prediction performance. We found non-significant correlations between them (r = 0.11, P = 0.4566 for the pain prediction, and r = 0.19, P = 0.1911 for the pleasure prediction). After excluding the outlier region, the primary somatosensory cortex (S1), the correlations were still non-significant: r = 0.28, P = 0.0610 for the pain prediction, and r = 0.21, P = 0.1519 for the pleasure prediction. Red circles indicate the 7 overlapping brain regions. Amyg: amygdala, aINSinf: insula anterior inferior cortex, pOFC: posterior orbitofrontal cortex, lPFC: lateral prefrontal cortex, mPFC: medial prefrontal cortex.

18
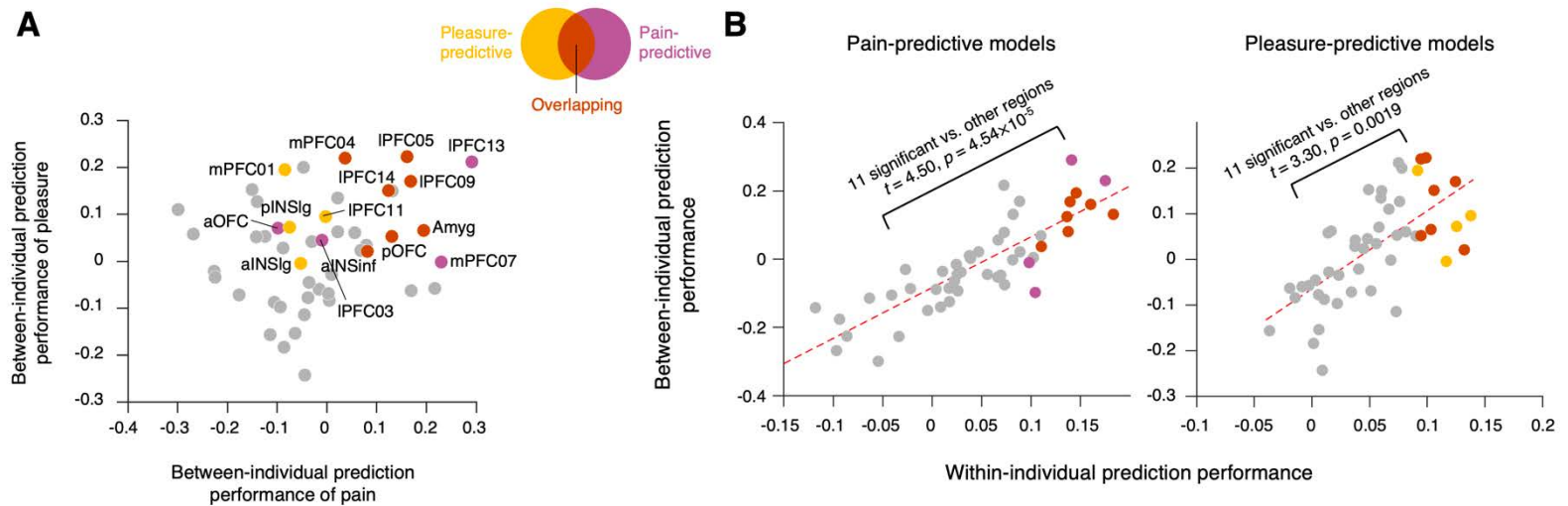
Fig. S9. Between-individual prediction performances of the region-level models; related to Fig. 2A). (A) We assessed how the 48 region-level pain- and pleasure-predictive models predicted the average ratings of each condition across individuals. For pain-predictive models, we calculated the prediction-outcome correlation across capsaicin and control conditions. For pleasure-predictive models, we calculated the correlation across chocolate and control conditions. We highlighted the regions that showed significant within-individual prediction performances (from **Fig. 2A**) using the same color scheme (purple: pain-predictive; yellow: pleasure-predictive; vermilion: overlapping). **(B)** Scatter plots that show the relationship between within- and between-individual prediction performances. Left: 48 region-level pain-predictive models (purple: pain-predictive; vermilion: overlapping). Right: 48 region-level pleasure-predictive models (yellow: pleasure-predictive; vermilion: overlapping).
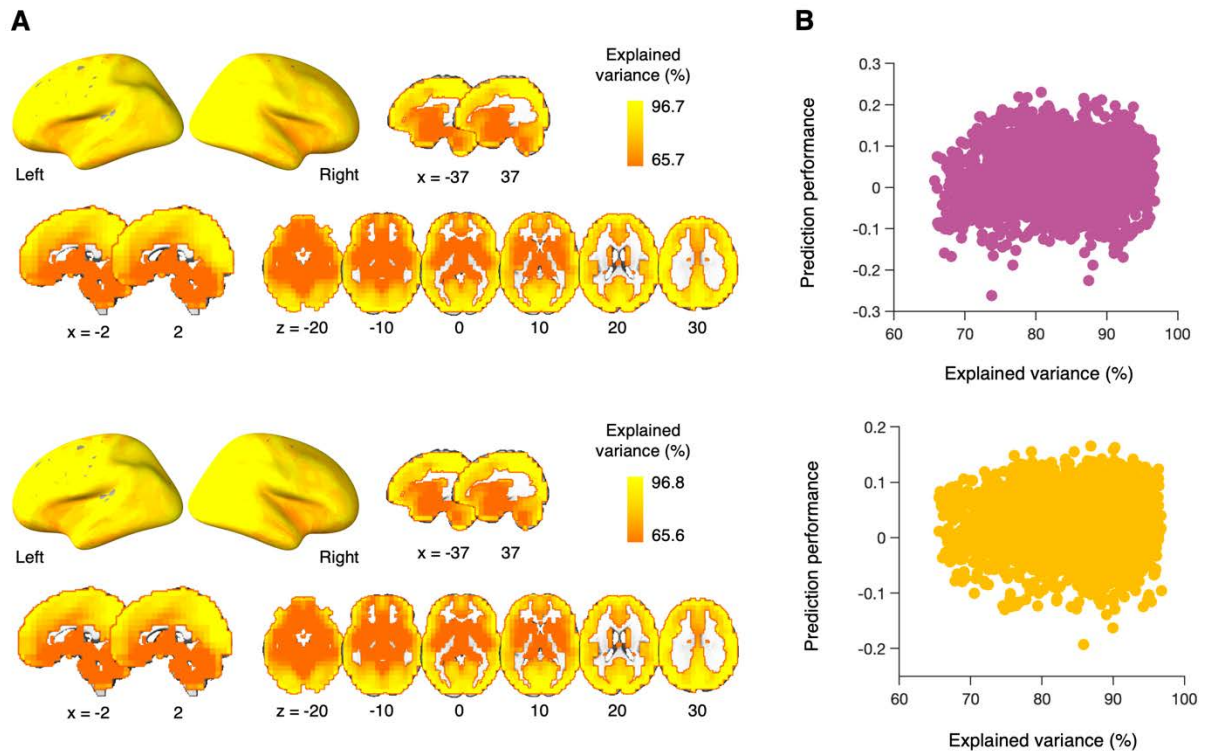
Fig. S10. Explained variances with 13 Principal Components (PCs) across searchlights (related to Fig. 2B). (A) The explained variance across searchlight regions based on 13 PCs. Top: for capsaicin and control data (range: 65.7-96.7%), bottom: for chocolate and control data (range: 65.6-96.8%). **(B)** The relationship between the explained variance and the prediction performance across searchlight regions. Purple: $r = 0.03$, $P = 0.0754$ for the pain prediction. Yellow: $r = -0.01$, $P = 0.4188$ for the pleasure prediction.
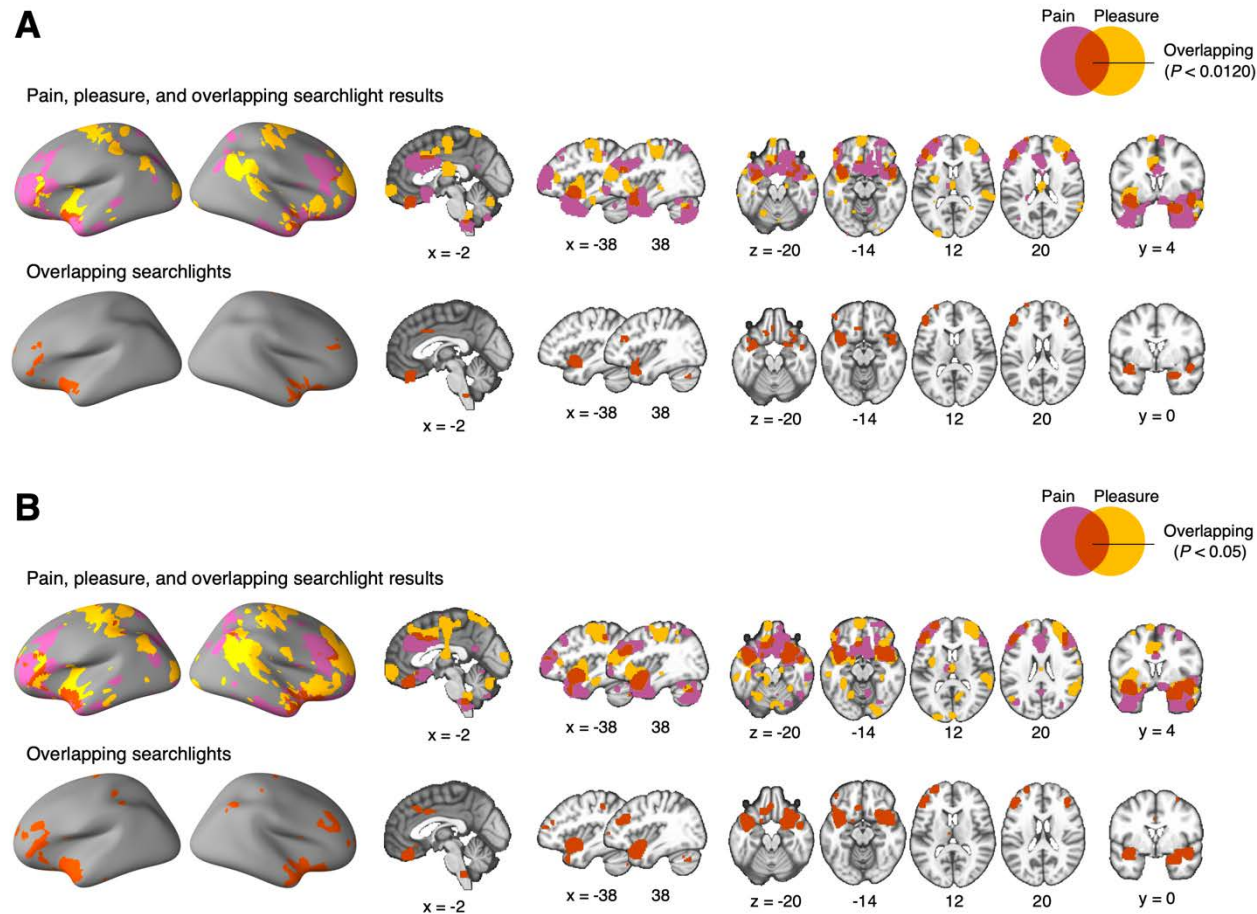
Fig. S11. Searchlight analysis results with similar numbers of voxels as shown in Fig. 2A (related to Fig. 2B). The maps are the same as Fig. 2B but **(A)** with the same thresholding level as Fig. 2A ($q < 0.05$, FDR corrected, corresponding to uncorrected $P < 0.0120$), and **(B)** with the top 12.91% of voxels (corresponding to uncorrected $P < 0.05$) that are similar numbers of voxels shown in Fig. 2A.

Fig. S12. Region-level predictive modeling for the capsaicin and control conditions with different numbers of principal components (related to Fig. 2A). Though we used 13 PCs for main analyses, we also tested different numbers of PCs to examine how robust our results were. We varied the number of PCs (8~23) with different levels of explained variance (i.e., 65%, 70%, 75%, 80%, and 85%) and examined which brain regions showed significant prediction performance in

predicting ratings for the capsaicin and control conditions. The brain maps show regions with significant prediction performance thresholded at FDR $q < 0.05$.

Brain regions with significant (FDR $q < 0.05$) performance in predicting ratings for the **chocolate** and control conditions

Prediction-outcome correlation

8 components (explained variance 65%)

10 components (explained variance 70%)

13 components (explained variance 75%)

17 components (explained variance 80%)

23 components (explained variance 85%)
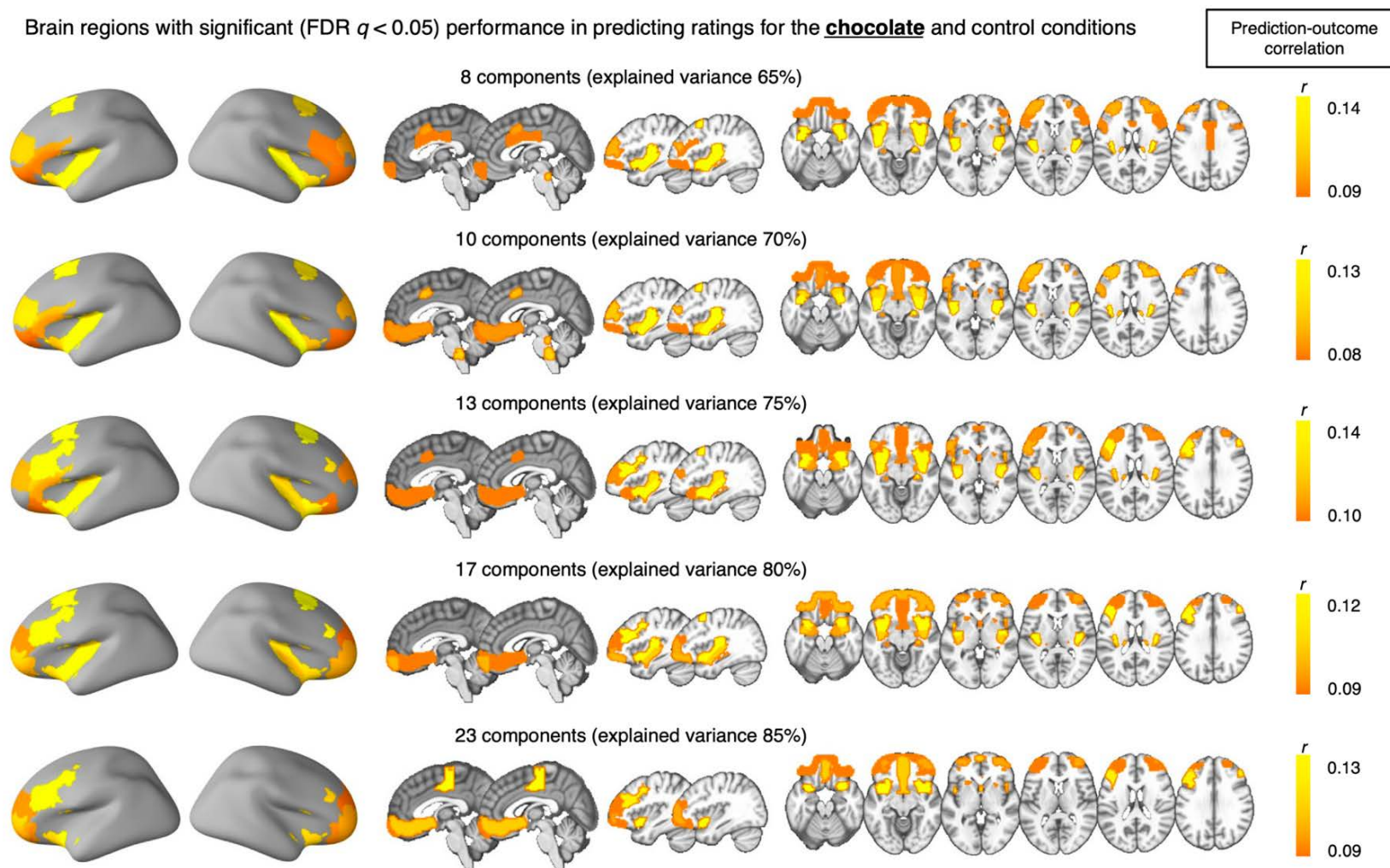
Fig. S13. Region-level predictive modeling for the chocolate and control conditions with different numbers of principal components (related to Fig. 2A**).** Same as **Fig. S11**, but the results of predicting ratings for the chocolate and control conditions.

A Distributions of ratings for each condition: before vs. after subsampling

Capsaicin   Chocolate   Control
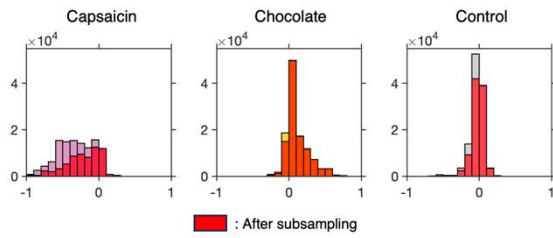
: After subsampling

B Distributions of timepoints of excluded ratings across conditions

Capsaicin
Chocolate
Control

1st delivery   2nd delivery

Time (mins)

Fig. S14. Rank-based subsampling of behavioral ratings. (related to Fig. 3) (A) Rating distributions before and after the subsampling process. **(B)** Distributions of the time points excluded by the subsampling process across all iterations of leave-one-participant-out cross-validation. In the capsaicin condition, time points associated with high unpleasantness rating scores were more prone to exclusion during the subsampling procedure.
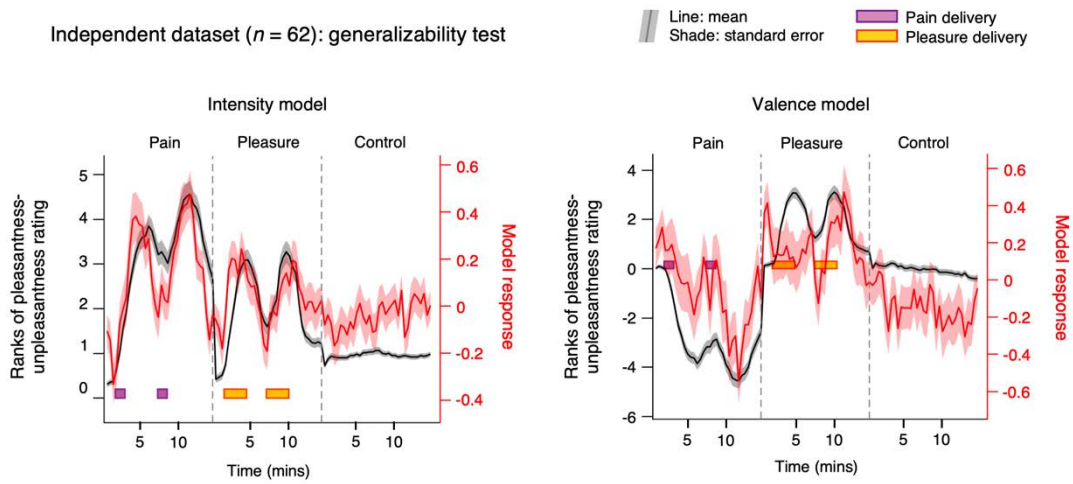
Fig. S15. Testing intensity and valence models on the independent dataset (Study 2, *n* = 62; related to Fig. 3). We tested whether the intensity and valence models also showed the time-course of pattern expression values similar to the overall trajectories of ratings, as we observed from the training dataset results. The solid line represents the group average, and the shading represents the standard error of the mean. The colored boxes indicate the fluid delivery period (purple for capsaicin and yellow for chocolate).
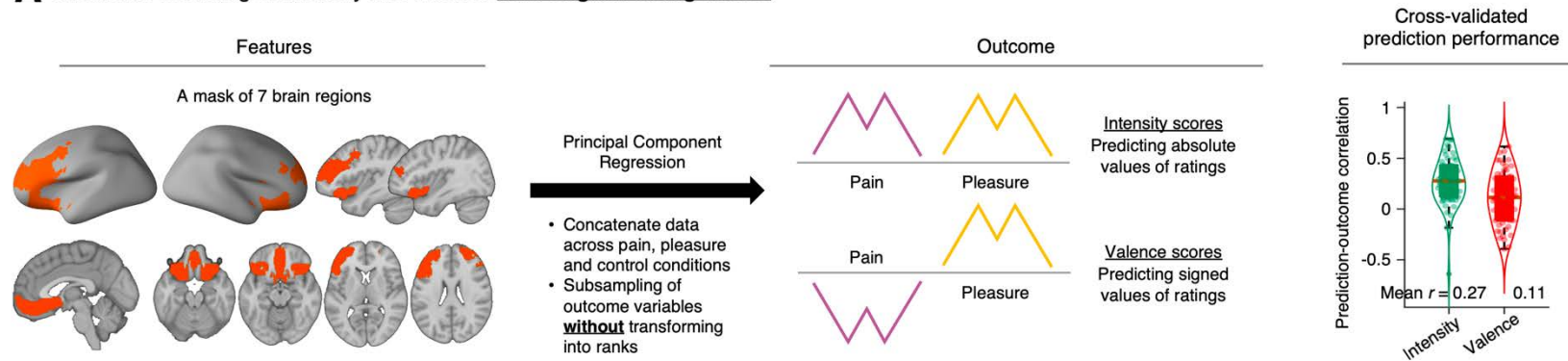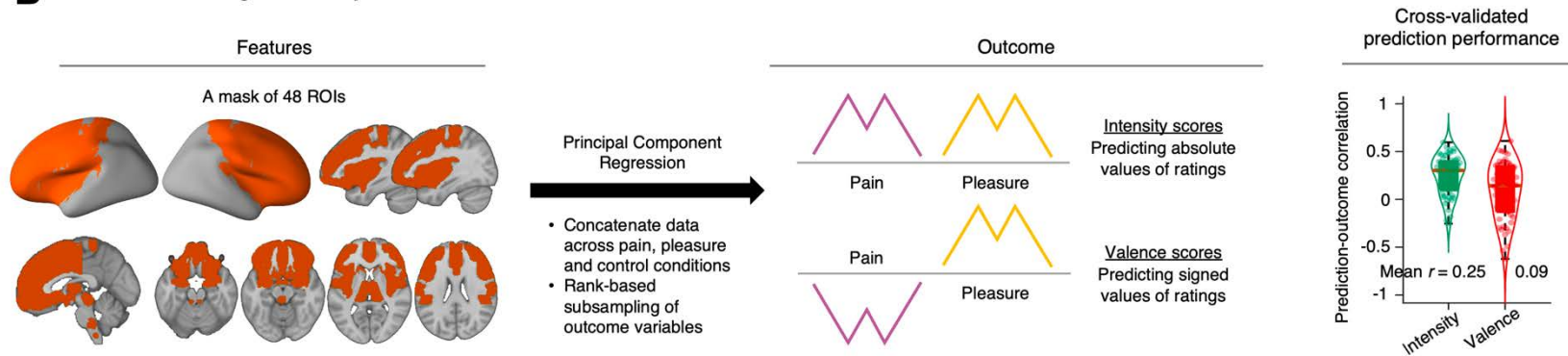
**Fig. S16. Predictive modeling of affective intensity and valence using original rating values and the whole 48 ROIs (related to Fig. 3). (A)** When we used the original rating values as the outcome, instead of the rank values, the mean within-individual prediction-outcome correlation for the intensity model was $r = 0.27$, $P = 2.22 \times 10^{-16}$, bootstrap test, two-tailed, mean of mean squared error (mse) = 0.0395, and for the valence model, $r = 0.11$, $P = 7.62 \times 10^{-4}$, bootstrap test, two-tailed, mean mse = 0.0651.

(B) When we used 48 ROIs instead of 7 ROIs, the mean within-individual prediction-outcome correlation for the intensity model was r = 0.25, $P < 2.22 \times 10^{-16}$, bootstrap test, two-tailed, mean mse = 13.225 and for the valence model, r = 0.09, P = 0.0232, bootstrap test, two-tailed, mean mse = 24.522.
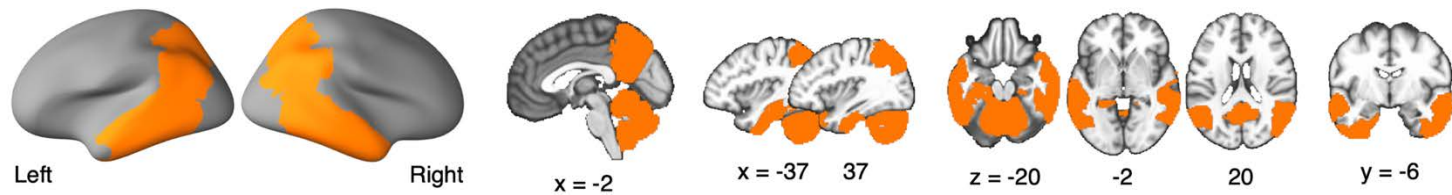
Fig. S17. A mask of 61 brain regions used for predictive modeling of the affective intensity and valence (related to Fig. 3). A spatial mask of 61 brain regions from the 265-region whole-brain parcellation combining Schaefer cortical atlas (4) with additional subcortical and cerebellar regions from the Brainnetome atlas (41) and brainstem regions (42, 43). We excluded the brain regions that had overlapping voxels more than 1% with the 48 ROIs and the visual network (44).
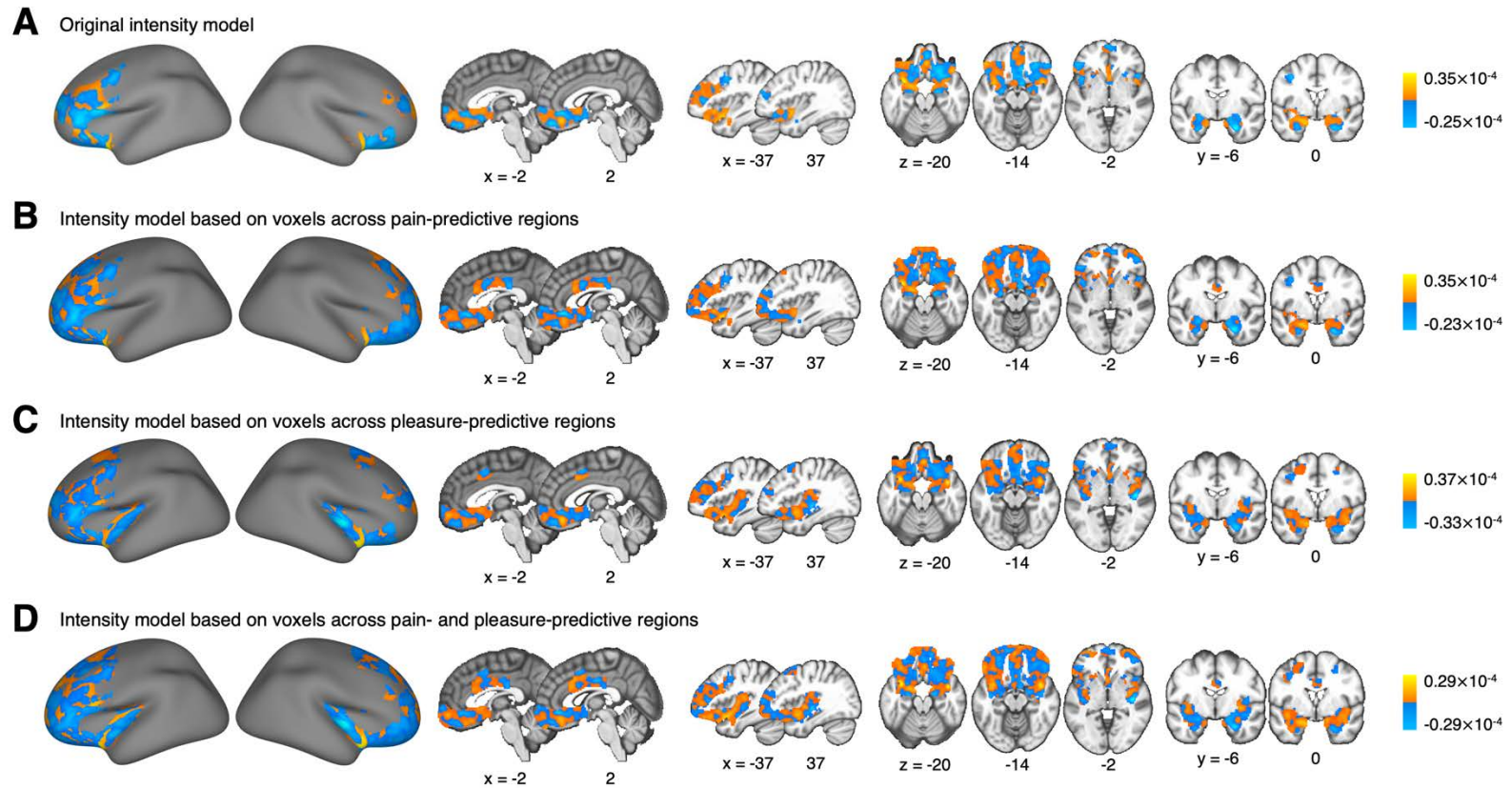
Fig. S18. Unthresholded weight maps across 3 intensity models. (related to Fig. 3) The unthresholded weights of the intensity models based on **(A)** the original 7 overlapping brain regions, **(B)** 11 pain-predictive brain regions, **(C)** 11 pleasure-predictive brain regions, and **(D)** all 15 significant brain regions. The spatial correlation of the predictive weights within the 7 overlapping brain regions between **(A)** and **(B)** was $r = 0.89$, $P = 2.22 \times 10^{-16}$, that between **(A)** and **(C)** was $r = 0.90$, $P = 2.22 \times 10^{-16}$, and that between **(A)** and **(D)** was $r = 0.83$, $P = 2.22 \times 10^{-16}$.
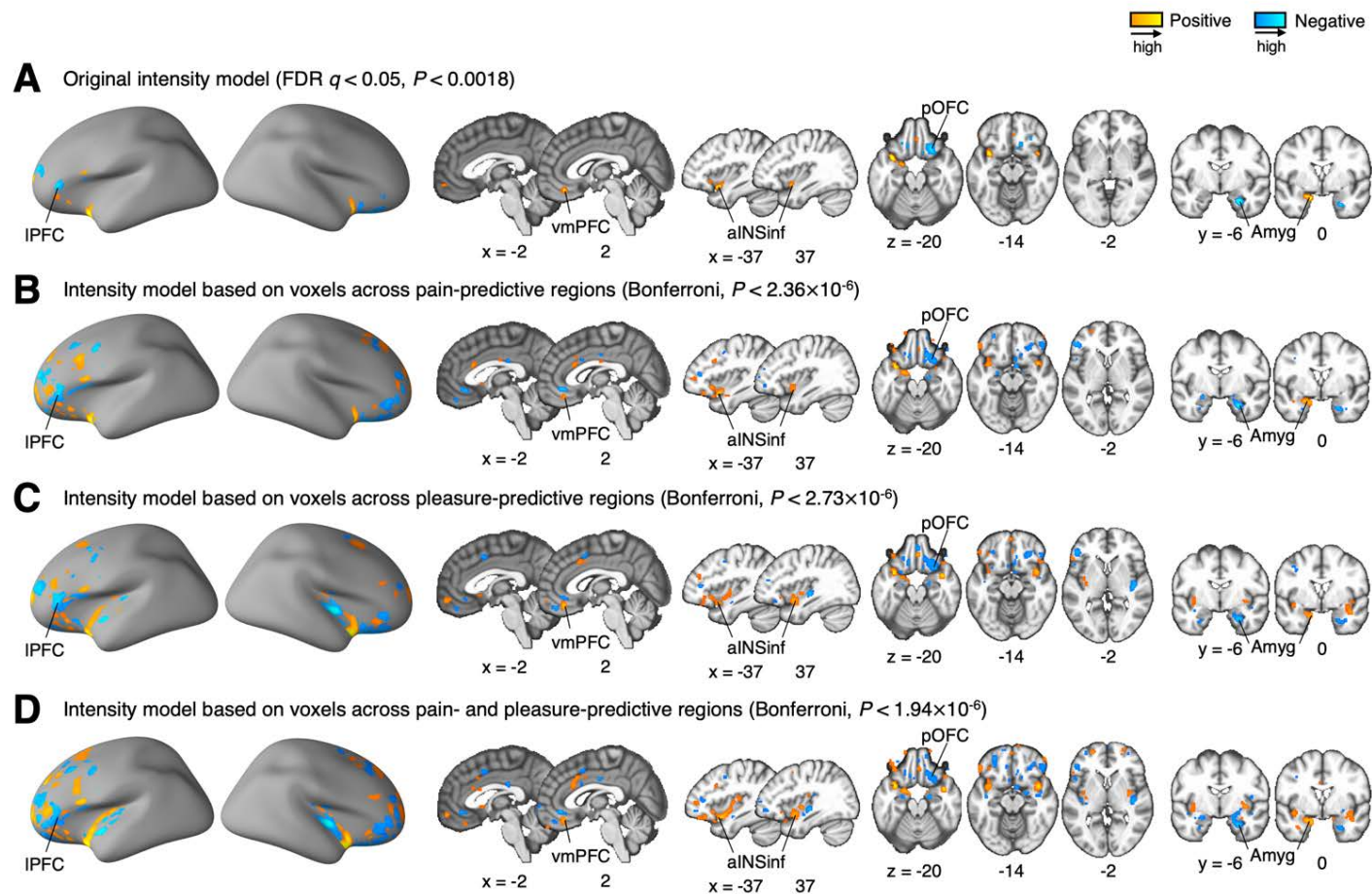
Fig. S19. Thresholded weight maps across 3 intensity models. (related to Fig. 3) Thresholded weights of the intensity models based on **(A)** the original 7 overlapping brain regions (FDR $q < 0.05$), **(B)** 11 pain-predictive brain regions (Bonferroni $p < 0.05$), **(C)** 11 pleasure-predictive brain regions (Bonferroni $p < 0.05$), and **(D)** all 15 significant brain regions (Bonferroni $p < 0.05$).
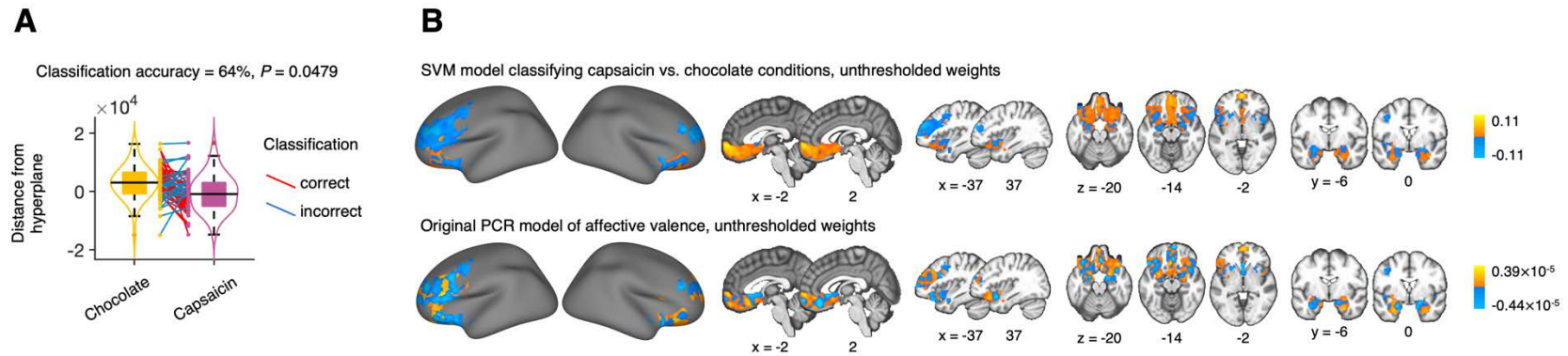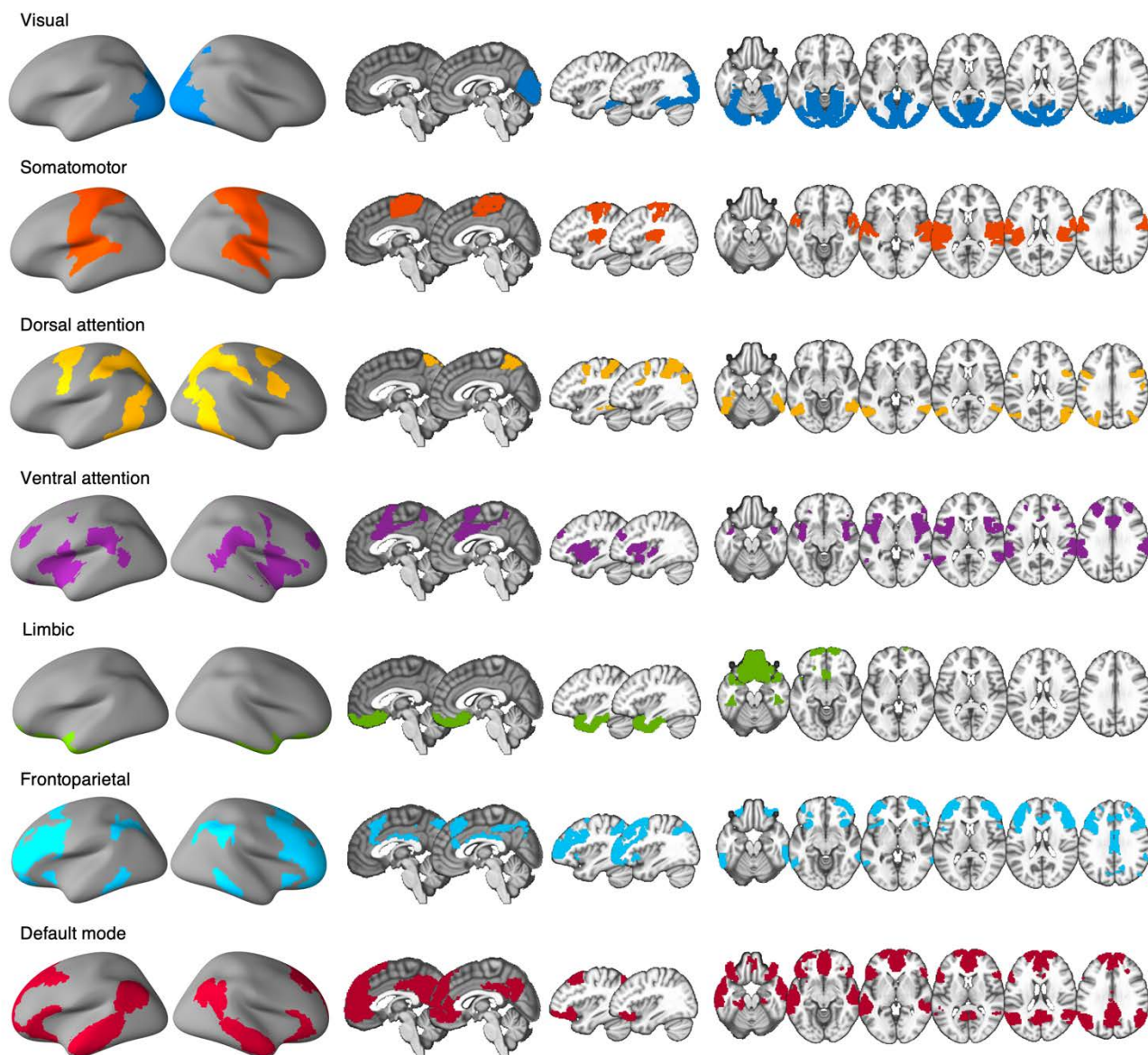
Fig. S20. The Support Vector Machine (SVM)-based classification model distinguishing the chocolate and capsaicin conditions based on the 7 overlapping brain regions. (A) The forced-choice test result based on leave-one-participant-out cross-validation. Each line connecting dots represents an individual participant's paired data (red line: correct classification, blue line: incorrect classification). *P*-value was based on a binomial test, two-tailed. **(B)** The unthresholded weights of the SVM model classifying capsaicin versus chocolate conditions and the original PCR-based valence model. The spatial correlation between these predictive weights was r = 0.41, P = 2.22×10^{-16}.
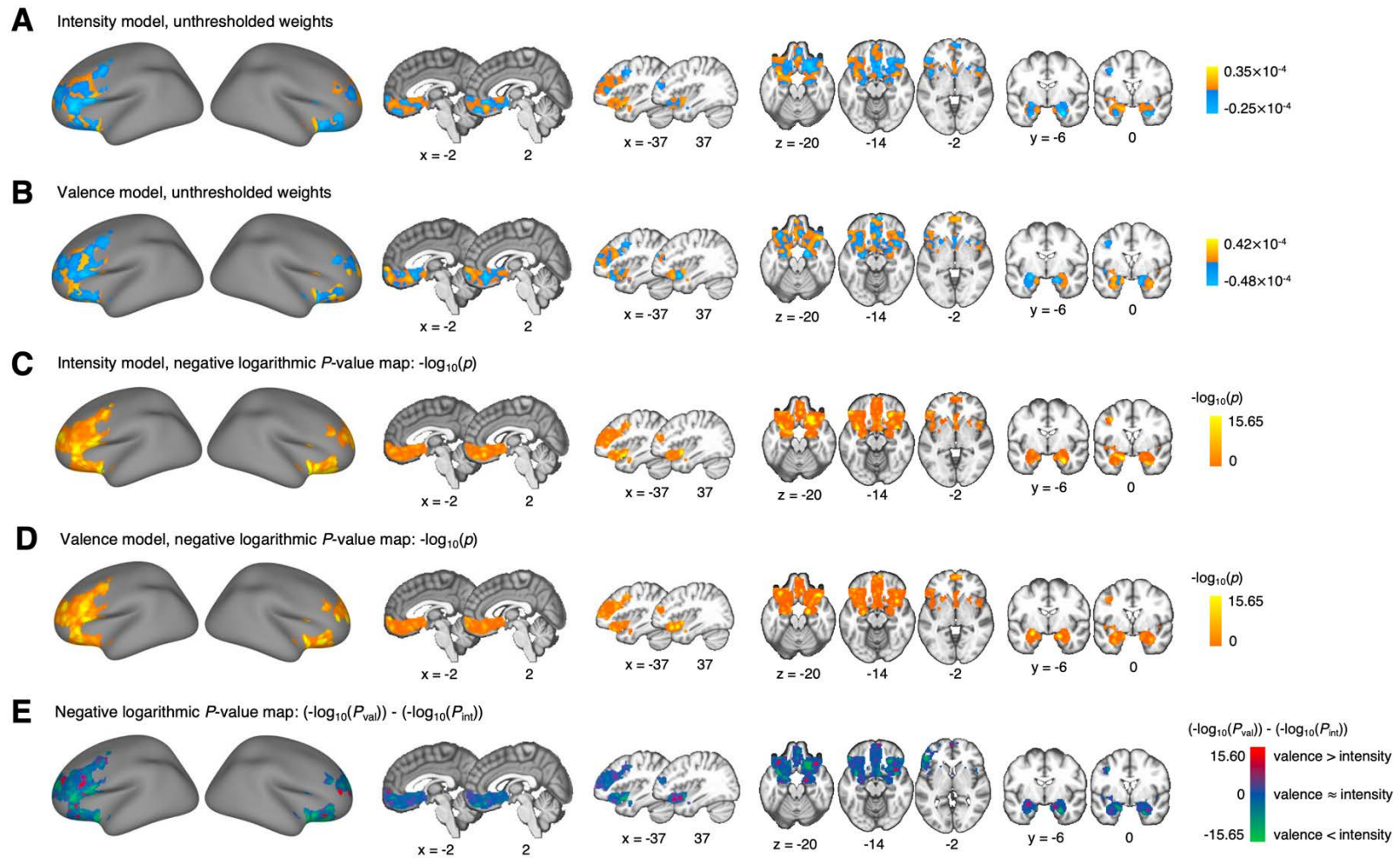
Fig. S21. Unthresholded predictive weights and their *P*-values of intensity and valence models (related to Fig. 3). (A-B) Unthresholded predictive weights of **(A)** the intensity model and **(B)** the valence model. **(C-E)** We obtained the *p*-values from

bootstrap tests with 10,000 iterations. Negative logarithmic of p-values of the unthresholded predictive weights of the **(C)** intensity model and **(D)** the valence model. **(E)** The relative importance of the voxels for the intensity versus valence models, defined as the difference of negative logarithmic of p-values of the unthresholded weights between the two models. Here we defined the importance of the voxels as the negative logarithmic of p-values to base 10 from bootstrap tests. The brain regions with lower p-values for the intensity model were colored green, and the brain regions with lower p-values for the valence model were colored red.

Visual

Somatomotor

Dorsal attention

Ventral attention

Limbic

Frontoparietal

Default mode

Fig. S22. Large-scale cortical functional networks. (related to Fig. 5) The 7 cortical functional networks from the Buckner group (44).
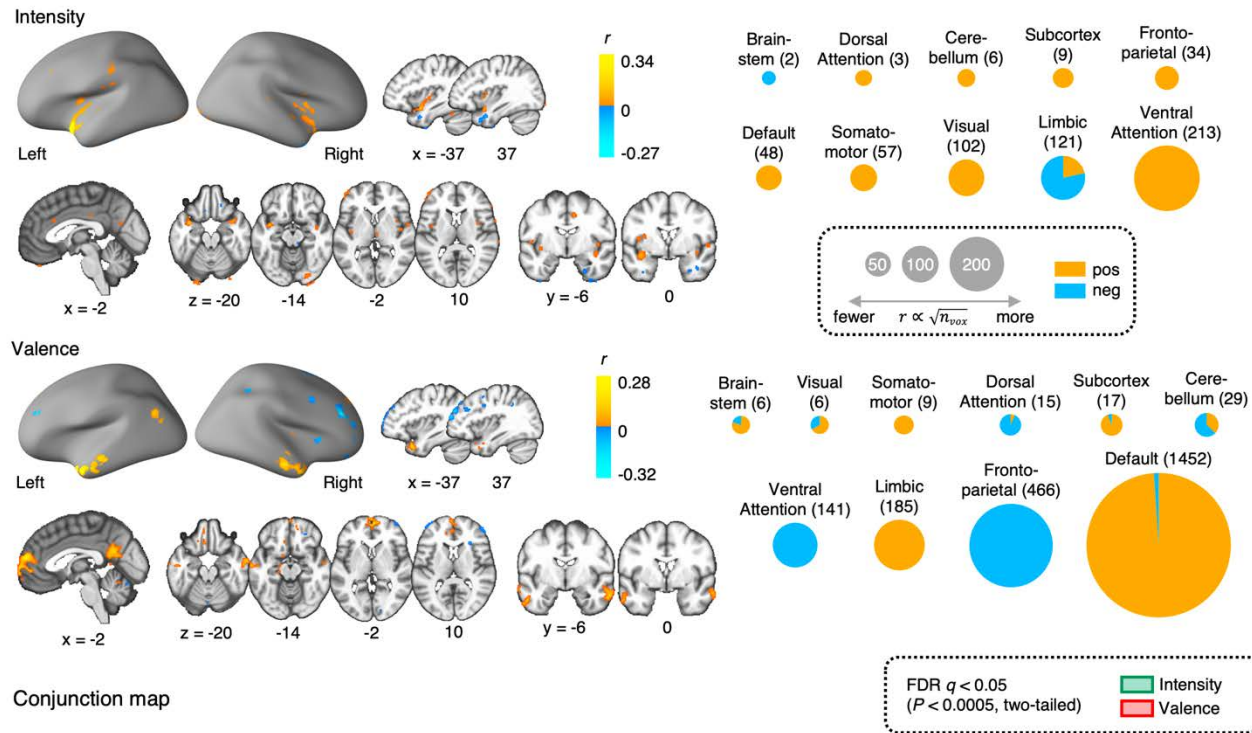
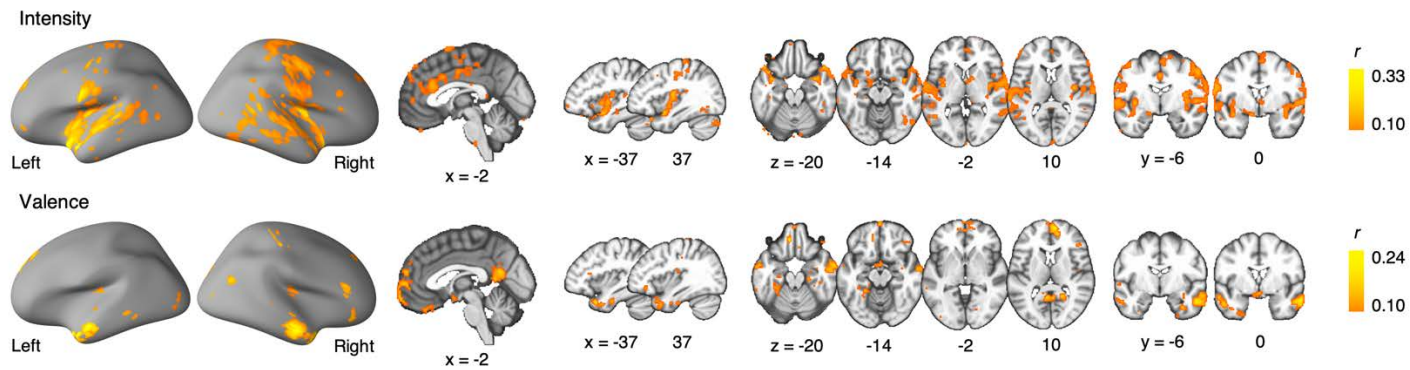**Fig. S23. Functional connectivity maps for the intensity and valence models including both positive and negative correlations (related to Fig. 5). (A)** Left: Thresholded functional connectivity maps of intensity and valence models including both

positive and negative correlation values (FDR $q < 0.05$, one-sample t-test, two-tailed). We excluded the brain coverage of the predictive models to focus on their relationship with other brain regions. Right: The pie charts showed the proportions of voxels that survived after thresholding given each large-scale functional brain network. The radius of each pie chart is proportional to the total number of voxels; the more voxels in each brain network survive, the bigger the pie chart is. The actual numbers of all survived voxels in each brain network are indicated in parentheses. **(B)** A conjunction map of the intensity and valence model-based connectivity maps; green for the intensity model and red for the valence model.
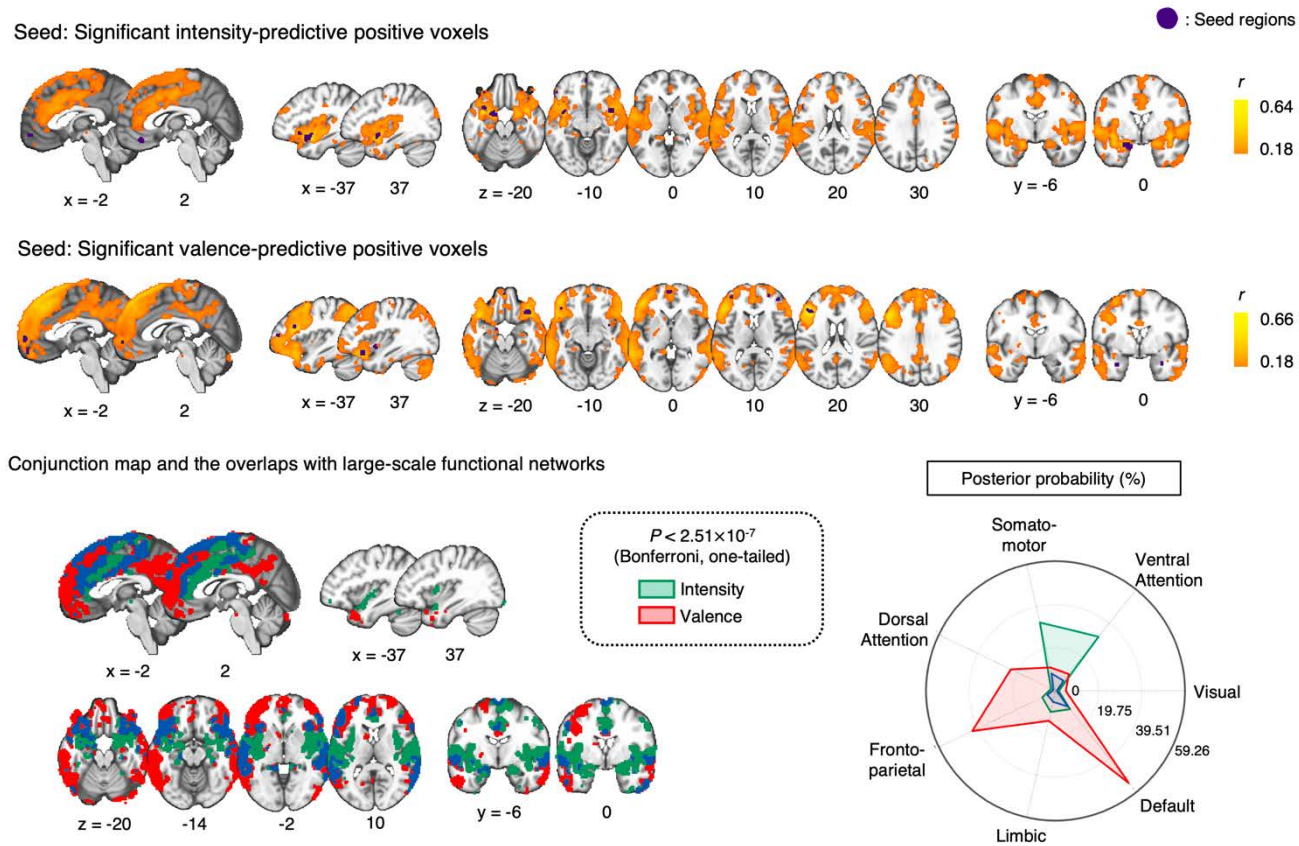
Fig. S24. Results of conventional seed-based functional connectivity analysis (related to Fig. 5). These plots show the group-level seed-based functional connectivity maps. We used the voxels colored in white with significant (at FDR $q < 0.05$, two-tailed, from bootstrap tests with 10,000 iterations) positive predictive weights from the intensity and valence models as a seed mask. Then, the average activation values across the mask were used to calculate functional connectivity with the control condition data. We showed only positive connectivity thresholded at Bonferroni-corrected $p < 0.05$ (voxel-wise $p < 2.51 \times 10^{-7}$).
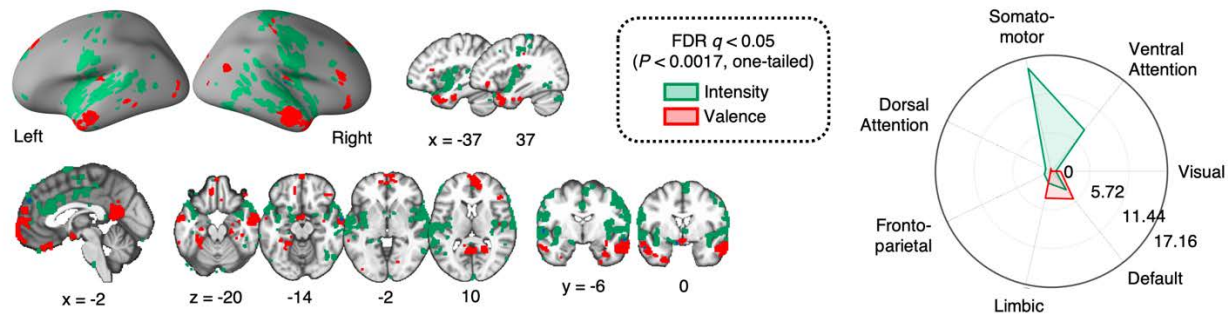
Fig. S25. Functional connectivity maps for the intensity and valence models on the independent dataset (Study 2, *N* = 62; related to Fig. 5). We obtained the functional connectivity using the pattern expression values of intensity and valence models as seeds in the independent dataset (Study 2, *N* = 62). The functional connectivity was calculated using the control condition data. **(A)** Thresholded functional connectivity patterns (FDR *q* < 0.05, one-sample *t*-test, one-tailed). **(B)** Left: Conjunction maps with different colors indicating the results of the different models—green for the intensity model and red for the valence model. Right: A radar plot

showing the posterior probability of the significant voxels within each large-scale functional network given the total number of voxels within each network.
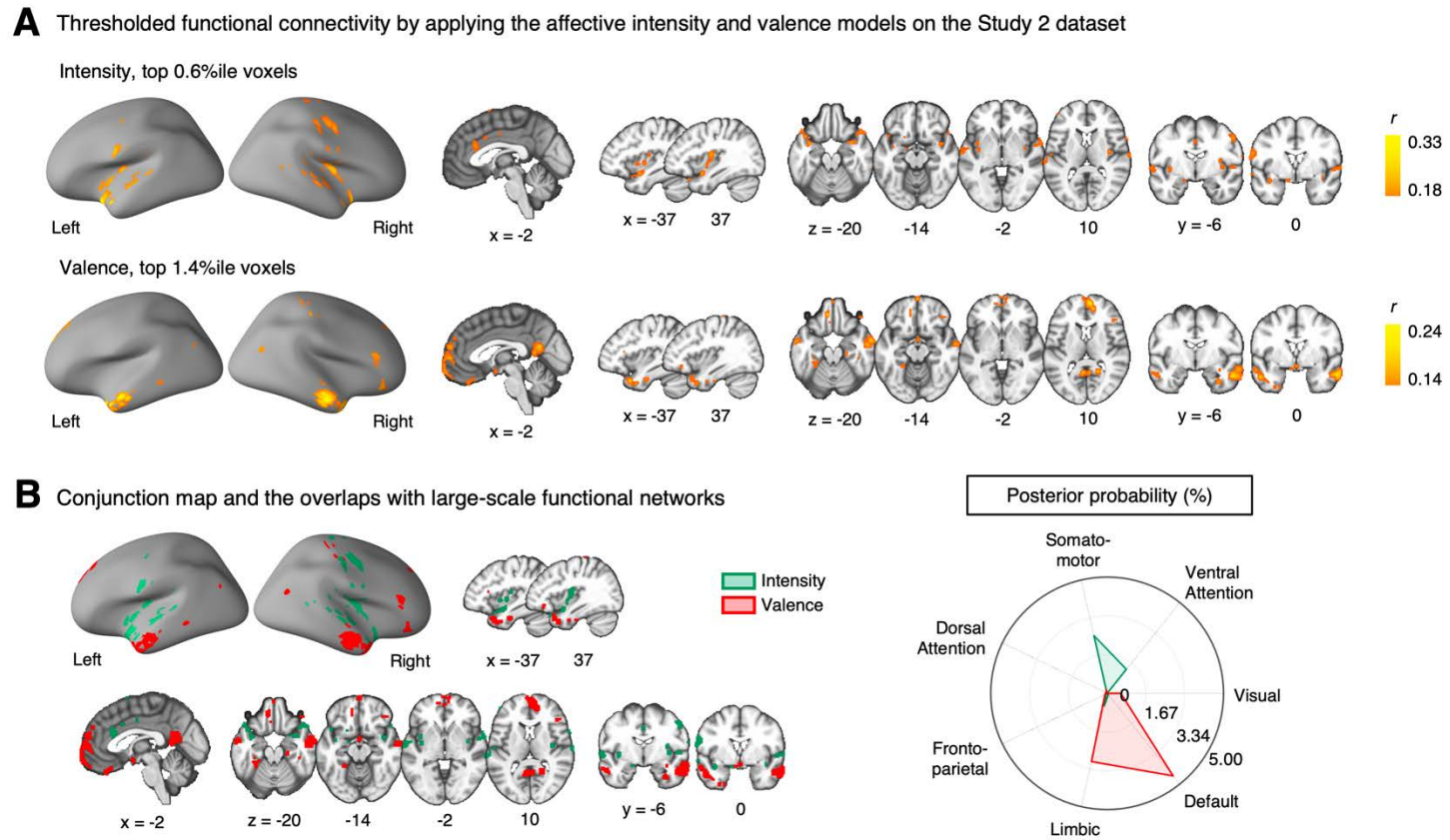
Fig. S26. Functional connectivity maps for the intensity and valence models on the independent dataset (Study 2, *N* = 62; related to Fig. 5). Same as **Fig. S25** but showing similar numbers of significant voxels as in **Fig. 5**. **(A)** Thresholded functional connectivity patterns with the top 0.6%ile (1,190 voxels) in the intensity and top 1.4%ile (2,776 voxels) in the valence. **(B)** Left: Conjunction maps with different colors indicating the results of the different models—green for the intensity model and red for the valence model. Right: A radar plot showing the posterior probability of the significant voxels within each large-scale functional

network given the total number of voxels within each network. Compared to **Fig. S25**, the functional connectivity for the intensity model showed stronger connection to the somatomotor network than the ventral attention network.
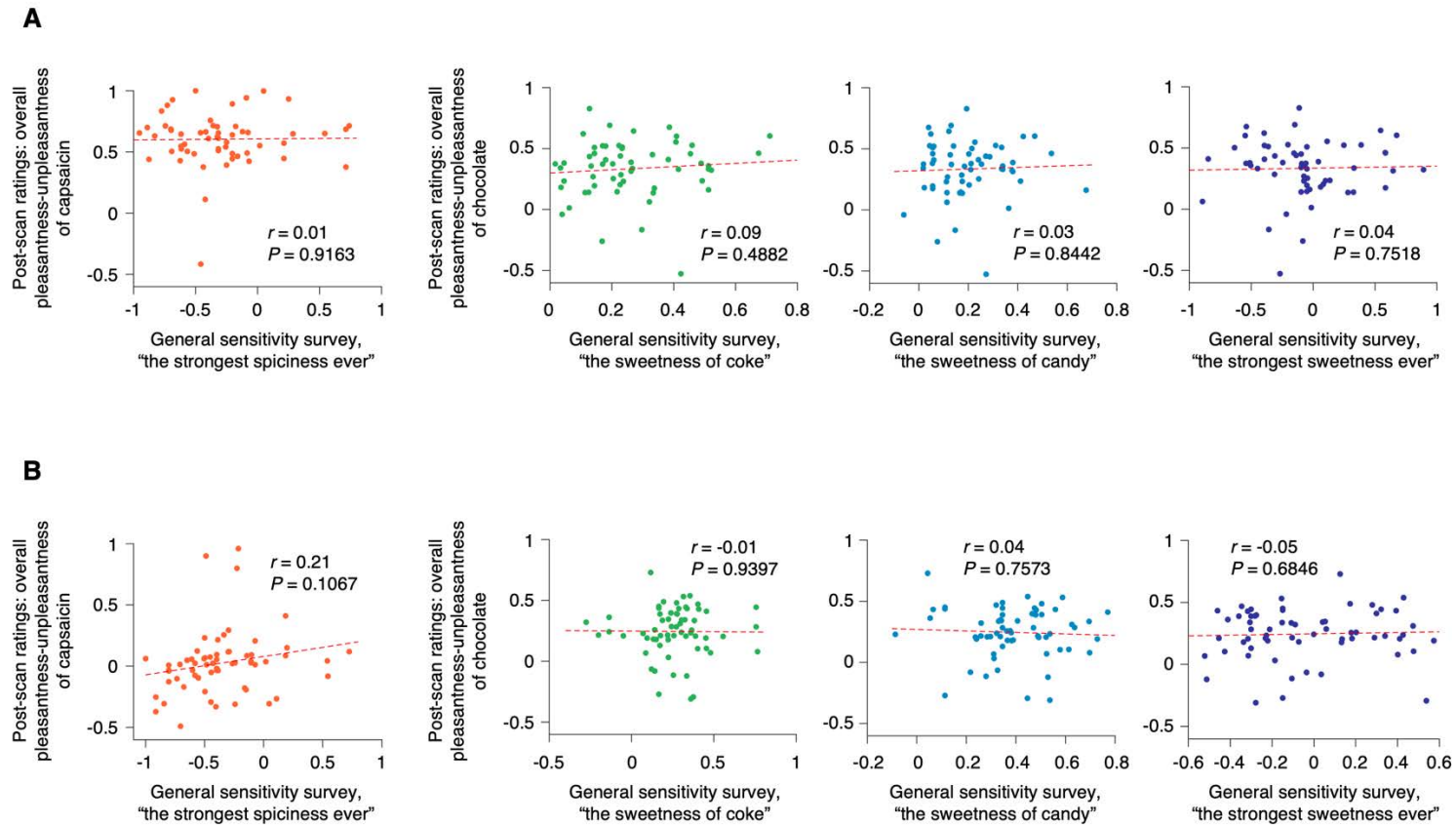
Fig. S27. Relationships between the participants' general sensitivity scores on the (un)pleasantness ratings for a variety of tastes and sensory stimuli (38, 45) and the overall (un)pleasantness ratings for capsaicin or chocolate stimuli after the fMRI experiments. We examined the relationships between participants' general sensitivity scores on various sensory stimuli before the fMRI experiments and overall (un)pleasantness ratings for capsaicin and chocolate stimuli after the fMRI experiments, across **(A)** Study 1 and **(B)** Study 2.
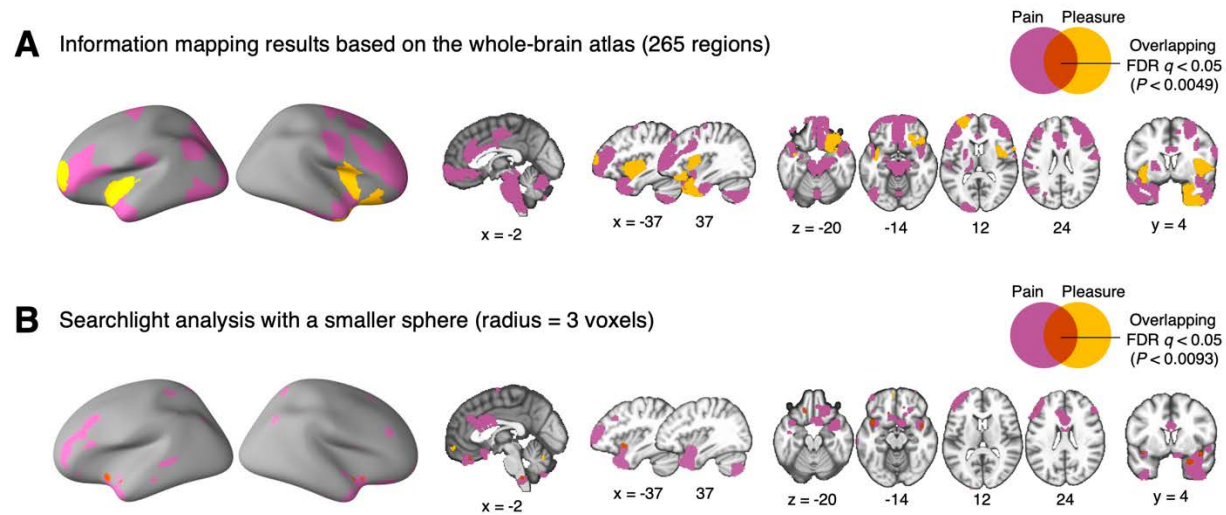
Fig. S28. Information mapping results with Schaefer parcellations (4) and smaller searchlights (related to Fig. 2B). (A) Brain regions that showed significant prediction performances (FDR *q* < 0.05) for the information mapping of pain and pleasure, using 265-region whole-brain parcellation combining Schaefer cortical atlas (4) with additional subcortical and cerebellum regions from the Brainnetome atlas (41) and brainstem regions (42, 43). **(B)** Searchlight voxels that showed significant prediction performances (FDR *q* < 0.05) with a reduced size (radius = 3 voxels; originally 5 voxels as in **Fig. 2B**).

A Regions correlated with ratings of the capsaicin condition (FDR $q < 0.05$, $P < 0.0002$)

dpINS

Left   Right $x = -37$ 37

Pain+
Pain-

$x = -2$ 2 $z = -20$ -10 0 10 20 $y = -6$ 0
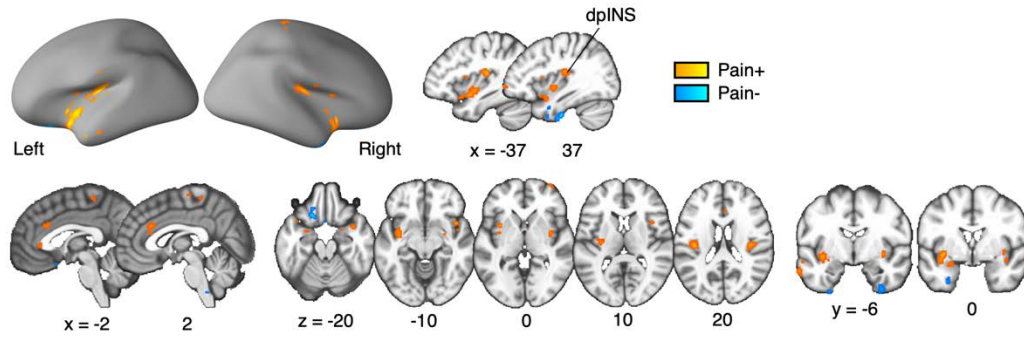
B Regions correlated with ratings of the chocolate condition (FDR $q < 0.05$, $P < 0.0002$)

Left   Right $x = -37$ 37

Pleasure+
Pleasure-

$x = -2$ 2 $z = -20$ -10 0 10 20 $y = -6$ 0
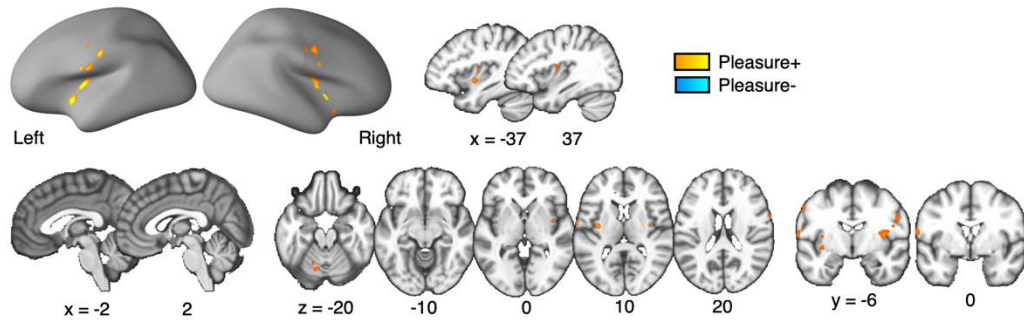
Fig. S29. Univariate GLM analysis using TR-level fMRI and pleasantness-unpleasantness ratings (related to Fig. 2). (A-B) To examine which voxels were correlated with the ratings during the capsaicin versus chocolate conditions, we conducted a univariate general linear modeling (GLM) analysis using TR-level fMRI and behavioral data. We used the TR-level pleasantness-unpleasantness ratings convolved with the canonical hemodynamic response function as a regressor for **(A)** the 'capsaicin' and **(B)** the 'chocolate' conditions. We also included the nuisance covariates (24 head motion parameters, linear drift, outlier indicators, and five principal components of white matter and ventricle signals) to remove nuisance effects in each fMRI condition. We then conducted one-sample *t*-tests for the beta coefficients with FDR correction for multiple comparisons.
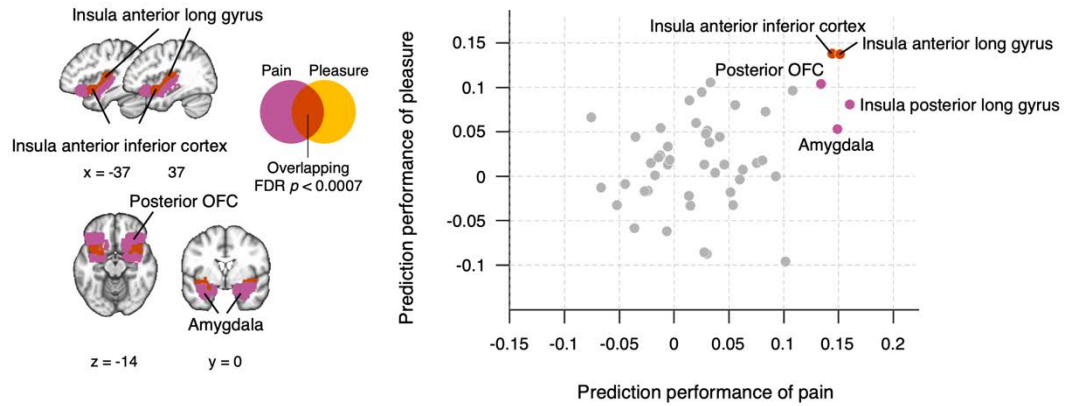
Fig. S30. ROI-level predictive modeling results based on the within-individual variability across 48 ROIs (related to Fig. 2). We trained individualized models and obtained the model weights for each individual. The prediction performance was estimated with leave-one-participant-out cross-validation, in which we averaged all models except for one individual and tested the averaged model on the remaining individual (we followed the modeling approach described in ref. (46)). We used the same 48 ROIs as in **Fig. 1C**.
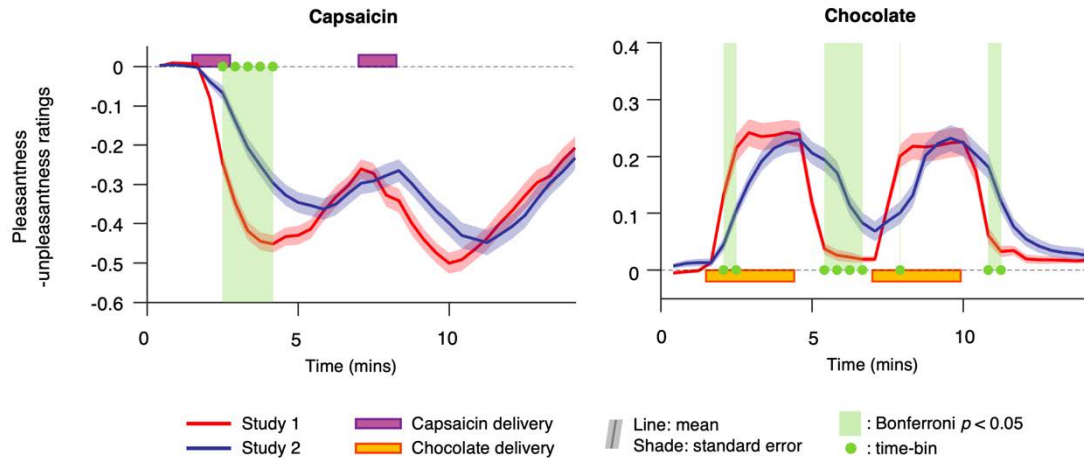
Fig. S31. Comparing patterns of pleasantness-unpleasantness ratings between Studies 1 and 2 (related to Figs. 1 and 2). The solid lines indicate group averages of pain and pleasure ratings (red for Study 1, blue for Study 2), and the shading indicates standard errors of the mean (s.e.m.). Purple boxes: capsaicin delivery, yellow boxes: chocolate delivery. Green boxes and dots indicate the time-bins that showed significant differences in behavioral ratings between Studies 1 and 2 (Bonferroni $p < 0.05$).

Table S1. Predicting affective intensity using individual 7 overlapping brain regions (related to Fig. 3).

Brain regions	All conditions			'Capsaicin' condition			'Chocolate' condition		
	mean r	P	mean mse	mean r	P	mean mse	mean r	P	mean mse
Amygdala	0.15	$2.24 \times 10^{-6*}$	13.545	0.20	0.0007^*	20.882	0.17	$1.22 \times 10^{-5*}$	15.311
Insula anterior inferior cortex	0.18	$9.03 \times 10^{-13*}$	13.402	0.23	$8.01 \times 10^{-6*}$	20.946	0.15	0.0004^*	15.123
lPFC05	0.11	0.0002^*	13.668	0.24	0.0001^*	20.947	0.04	0.2747	15.644
lPFC09	0.07	0.0249	13.729	0.10	0.3723	20.870	0.002	0.8506	15.704
lPFC14	0.13	$1.25 \times 10^{-5*}$	13.589	0.16	0.0028^*	20.802	0.07	0.0881	15.327
mPFC04	0.11	0.0002^*	13.710	0.16	0.0050	21.149	0.09	0.0312	15.495
Posterior OFC	0.15	$8.58 \times 10^{-7*}$	13.444	0.24	$2.56 \times 10^{-5*}$	20.977	0.17	0.0006	15.000

Note. The procedure of predictive modeling using each of the 7 brain regions was identical to that of using all 7 brain regions. The number of PCs that explained 75% of the total variance across 7 brain regions was 31, also an identical procedure used in the region-level information mapping. We trained the predictive models for each brain region by subsampling and transforming the individual rating data into ranks (±1~10; see **Materials and Methods**). lPFC: lateral prefrontal cortex, mPFC: medial prefrontal cortex, OFC: orbitofrontal cortex. mse: mean squared error. *FDR-corrected $q < 0.05$, bootstrap test, two-tailed.

Table S2. Predicting affective valence using individual 7 overlapping brain regions (related to Fig. 3).

Brain regions	All conditions			'Capsaicin' condition			'Chocolate' condition		
	mean r	P	mean mse	mean r	P	mean mse	mean r	P	mean mse
Amygdala	0.05	0.1907	23.927	0.03	0.5882	37.414	0.04	0.2708	27.179
Insula anterior inferior cortex	0.07	0.0577	24.031	-0.03	0.4457	37.070	0.07	0.1296	26.903
lPFC05	0.12	0.0002*	23.743	0.19	0.0008*	35.975	0.04	0.4761	27.205
lPFC09	0.12	0.0020*	23.604	0.21	0.0005*	35.917	-0.01	0.7183	26.541
lPFC14	0.10	0.0171	23.827	0.14	0.0099	36.395	0.05	0.2306	26.858
mPFC04	0.06	0.0851	23.829	0.02	0.6802	36.926	0.04	0.3780	26.869
Posterior OFC	0.06	0.0773	23.890	0.08	0.5199	36.761	0.06	0.1815	27.335

Note. Same as **Table S1**, but the results of affective valence prediction. lPFC: lateral prefrontal cortex, mPFC: medial prefrontal cortex, OFC: orbitofrontal cortex. mse: mean squared error. *FDR-corrected $q < 0.05$, bootstrap test, two-tailed.

Table S3. Numbers of voxels and the explained variance across 48 ROIs (related to Fig. 2).

Region names	Number of voxels	Explained variance (%)									
		8 PCs		10 PCs		13 PCs		17 PCs		23 PCs	
		Capsaicin & Control	Chocolate & Control	Capsaicin & Control	Chocolate & Control	Capsaicin & Control	Chocolate & Control	Capsaicin & Control	Chocolate & Control	Capsaicin & Control	Chocolate & Control
Amyg	1363	53	55	58	60	64	65	70	71	77	78
Hypothal	423	63	62	69	68	76	75	82	82	88	88
aINSinf	1825	53	52	57	56	62	61	67	67	74	74
aINSlg	1584	47	50	51	54	57	60	63	66	70	73
aINSsg	1642	53	52	57	56	62	61	67	67	74	74
mINSsg	865	59	59	64	64	69	70	75	75	81	81
pINSlg	1931	44	47	49	51	54	56	60	62	67	69
pINSsg	1107	57	57	61	61	67	67	72	73	79	79
lPFC01	2328	64	64	69	68	74	73	78	78	84	84
lPFC02	2056	71	68	74	73	79	77	83	82	87	86
lPFC03	1495	67	68	72	72	76	76	81	81	85	86
lPFC04	1380	66	64	70	69	75	74	80	79	85	85
lPFC05	2394	62	65	66	68	71	73	76	78	81	83
lPFC06	819	77	77	81	81	85	85	88	89	92	92
lPFC07	1530	66	65	70	69	75	74	80	79	85	85
lPFC08	1732	68	68	72	72	77	76	81	81	86	86
lPFC09	1709	67	65	71	69	76	74	80	79	85	84
lPFC10	1578	71	70	74	74	79	79	83	83	87	87
lPFC11	1259	72	72	75	76	80	80	84	84	88	88
lPFC12	932	77	76	81	80	84	84	87	87	91	91
lPFC13	1522	68	66	71	70	76	75	80	80	85	84
lPFC14	1379	69	69	73	73	77	78	82	82	86	87
mPFC01	441	81	84	85	87	88	90	92	93	95	95
mPFC02	1245	68	65	72	70	76	74	80	79	85	84
mPFC03	1401	65	68	69	71	74	76	78	80	83	85
mPFC04	2274	56	57	59	60	64	65	69	70	75	76
mPFC05	688	79	79	82	83	86	86	89	89	92	93
mPFC06	1842	72	69	75	73	79	77	83	81	87	86
mPFC07	1039	64	65	68	69	73	74	78	79	83	84
mPFC08	553	79	81	82	84	86	88	90	91	94	94
mPFC09	488	85	87	88	90	91	92	93	94	96	96
mPFC10	393	83	85	87	88	90	91	93	94	96	96
mPFC11	1300	71	70	75	74	79	78	83	82	87	87
mPFC12	880	71	72	75	76	79	80	84	85	89	89
NAc	397	68	67	73	72	79	78	84	84	90	90
NTS	154	88	87	90	90	93	93	96	96	98	98

aOFC	4513	49	50	53	54	58	59	64	64	70	71
pOFC	3452	51	50	55	53	59	59	65	64	71	70
aOper	776	66	66	70	71	75	76	80	81	86	86
mOper	2339	60	62	64	65	68	69	73	74	78	79
pOper	1289	67	69	70	72	75	77	80	81	85	86
PAG	337	68	68	73	73	80	80	86	85	91	91
PBN	189	72	74	78	79	84	84	89	90	94	94
RVM	339	66	67	72	73	78	79	84	85	90	91
S1	8982	62	62	65	65	69	69	74	73	78	78
Thal	2639	39	43	43	47	49	52	55	58	63	66
VeP	103	83	83	88	88	92	92	95	95	98	98
vStr	1220	50	48	55	53	61	59	67	65	75	73

Note. The 15 significant brain regions are highlighted using the same color scheme as used in Fig. 2A (purple: pain-predictive; yellow: pleasure-predictive; vermilion: overlapping). Amyg: amygdala, Hypothal: hypothalamus, aINSinf: insula anterior inferior cortex, aINSlg: insula anterior long gyrus, aINSsg: insula anterior short gyrus, mINSsg: insula middle short gyrus, pINSlg: insula posterior long gyrus, pINSsg: insula posterior short gyrus, lPFC: lateral prefrontal cortex, mPFC: medial prefrontal cortex, NAc: nucleus accumbens, NTS: nucleus of the solitary tract, aOFC: anterior orbitofrontal cortex, pOFC: posterior orbitofrontal cortex, aOper: anterior operculum, mOper: middle operculum, pOper: posterior operculum, PAG: periaqueductal gray, PBN: parabrachial nucleus, RVM: rostral ventral medulla, S1: primary somatosensory cortex, Thal: thalamus, VeP: ventral pallidum, vStr: ventral striatum.

Table S4. Results of information mapping analysis after excluding participants who had some issues in their rating patterns (related to Fig. 2).

Region names	Pain prediction			Pleasure prediction		
	Mean r	P	Mean mse	Mean r	P	Mean mse
Overlapping						
Amygdala	**0.14**	**0.0017***	**0.0498**	**0.11**	**0.0096***	**0.0202**
Insula anterior inferior cortex	**0.17**	**$3.48×10^{-5}$***	**0.0493**	**0.13**	**0.0023***	**0.0202**
lPFC05	**0.17**	**$7.96×10^{-6}$***	**0.0489**	**0.11**	**0.0039***	**0.0200**
lPFC09	**0.13**	**0.0009***	**0.0491**	**0.12**	**0.0025***	**0.0201**
lPFC14	**0.14**	**0.0006***	**0.0494**	**0.08**	**0.0564**	**0.0204**
mPFC04	**0.15**	**0.0001***	**0.0495**	**0.10**	**0.0005***	**0.0201**
Posterior OFC	**0.21**	**$6.06×10^{-7}$***	**0.0486**	**0.09**	**0.0370**	**0.0203**
Pain-predictive						
lPFC03	**0.06**	**0.0906**	**0.0509**	0.06	0.0802	0.0204
lPFC13	**0.12**	**0.0035***	**0.0494**	0.08	0.0677	0.0202
mPFC07	**0.17**	**$1.40×10^{-5}$***	**0.0496**	0.09	0.0138	0.0206
Anterior OFC	**0.15**	**0.0006***	**0.0499**	0.08	0.0205	0.0201
Pleasure-predictive						
Insula anterior long gyrus	0.06	0.0906	0.0513	**0.12**	**0.0114***	**0.0204**
Insula posterior long gyrus	0.04	0.3914	0.0518	**0.12**	**0.0012***	**0.0204**
lPFC11	0.09	0.0308	0.0506	**0.15**	**$4.08×10^{-5}$***	**0.0203**
mPFC01	0.004	0.9316	0.0513	**0.07**	**0.0867**	**0.0203**

Note. We excluded participants #005, 026, 029, 034, and 048 for pain prediction, and excluded participants #034, 039, 042, 048, and 056 for pleasure prediction. The procedure of information mapping was identical to that used for Fig. 2A. The number of PCs that explained 75% of the total variance across 48 brain regions based on 53 participants was 13. Prediction performances of brain regions relevant to either pain or pleasure prediction are highlighted in bold. Amyg: amygdala, OFC: orbitofrontal cortex, lPFC: lateral prefrontal cortex, mPFC: medial prefrontal cortex. *FDR $q < 0.05$, bootstrap test, two-tailed.

Table S5. Maximum levels of pleasantness-unpleasantness ratings of chocolate conditions in Studies 1 and 2 (related to Figs. 1 and 2).

Labels on gLMS	Study 1 (N [%])	Study 2 (N [%])
Very strong (0.533)	11 [19.0%]	6 [9.7%]
Strong (0.354)	25 [43.1%]	24 [38.7%]
Moderate (0.172)	51 [87.9%]	48 [77.4%]
Weak (0.061)	55 [94.8%]	57 [91.9%]

Note. gLMS: general Labels Magnitude Scale. Study 1: n = 58, Study 2: n = 62.

SI References

1. A. R. Segerdahl, M. Mezue, T. W. Okell, J. T. Farrar, I. Tracey, The dorsal posterior insula subserves a fundamental role in human pain. *Nat Neurosci* **18**, 499-500 (2015).
2. S. Geuter, S. Boll, F. Eippert, C. Büchel, Functional dissociation of stimulus intensity encoding and predictive coding of pain in the insula. *eLife* **6** (2017).
3. K. D. Davis, M. C. Bushnell, G. D. Iannetti, K. S. Lawrence, R. Coghill, Evidence against pain specificity in the dorsal posterior insula. *F1000Research* **4** (2015).
4. A. Schaefer *et al.*, Local-Global Parcellation of the Human Cerebral Cortex from Intrinsic Functional Connectivity MRI. *Cerebral Cortex* **28**, 3095-3114 (2018).
5. B. A. Kimmey, N. M. McCall, L. M. Wooldridge, T. D. Satterthwaite, G. Corder, Engaging endogenous opioid circuits in pain affective processes. *J Neurosci Res* 10.1002/jnr.24762 (2020).
6. J. O'Doherty, M. L. Kringelbach, E. T. Rolls, J. Hornak, C. Andrews, Abstract reward and punishment representations in the human orbitofrontal cortex. *Nat Neurosci* **4**, 95-102 (2001).
7. D. A. Seminowicz, M. Moayedi, The Dorsolateral Prefrontal Cortex in Acute and Chronic Pain. *J Pain* **18**, 1027-1035 (2017).
8. I. Gordon *et al.*, Brain mechanisms for processing affective touch. *Human Brain Mapping* **34**, 914-922 (2013).
9. F. Grabenhorst, E. T. Rolls, Value, pleasure and choice in the ventral prefrontal cortex. *Trends in Cognitive Sciences* **15**, 56-67 (2011).
10. J. Chikazoe, D. H. Lee, N. Kriegeskorte, A. K. Anderson, Population coding of affect across stimuli, modalities and individuals. *Nature Neuroscience* **17**, 1114-1122 (2014).
11. O. Bartra, J. T. McGuire, J. W. Kable, The valuation system: A coordinate-based meta-analysis of BOLD fMRI experiments examining neural correlates of subjective value. *NeuroImage* **76**, 412-427 (2013).
12. Z. Zhang *et al.*, Distributed neural representation of saliency controlled value and category during anticipation of rewards and punishments. *Nat Commun* **8**, 1907 (2017).
13. F. Grabenhorst, E. T. Rolls, B. A. Parris, A. A. d'Souza, How the Brain Represents the Reward Value of Fat in the Mouth. *Cerebral Cortex* **20**, 1082-1091 (2010).
14. F. Grabenhorst, E. T. Rolls, C. Margot, M. A. A. P. da Silva, M. I. Velazco, How Pleasant and Unpleasant Stimuli Combine in Different Brain Regions: Odor Mixtures. *Journal of Neuroscience* **27**, 13532-13540 (2007).
15. E. Kross, M. G. Berman, W. Mischel, E. E. Smith, T. D. Wager, Social rejection shares somatosensory representations with physical pain. *Proc Natl Acad Sci U S A* **108**, 6270-6275 (2011).
16. B. Horing, C. Sprenger, C. Buchel, The parietal operculum preferentially encodes heat pain and not salience. *PLoS Biol* **17**, e3000205 (2019).
17. D. M. Small, R. J. Zatorre, A. Dagher, A. C. Evans, M. Jones-Gotman, Changes in brain activity related to eating chocolate: from pleasure to aversion. *Brain* **124**, 1720-1733 (2001).
18. A. I. Basbaum, D. M. Bautista, G. Scherrer, D. Julius, Cellular and molecular mechanisms of pain. *Cell* **139**, 267-284 (2009).
19. D. D. Price, Psychological and neural mechanisms of the affective dimension of pain. *Science* **288**, 1769-1772 (2000).
20. C. B. Saper, The Central Autonomic Nervous System: Conscious Visceral Perception and Autonomic Pattern Generation. *Annual Review of Neuroscience* **25**, 433-469 (2002).
21. M. C. Bushnell, M. Čeko, L. A. Low, Cognitive and emotional control of pain and its disruption in chronic pain. *Nature Reviews Neuroscience* **14**, 502-511 (2013).
22. I. Tracey, Getting the pain you expect: mechanisms of placebo, nocebo and reappraisal effects in humans. *Nat Med* **16**, 1277-1283 (2010).
23. Kent C. Berridge, Morten L. Kringelbach, Pleasure Systems in the Brain. *Neuron* **86**, 646-664 (2015).

24.   D. C. Castro, K. C. Berridge, Advances in the neurobiological bases for food 'liking' versus 'wanting'. *Physiol Behav* **136**, 22-30 (2014).

25.   K. C. Berridge, M. L. Kringelbach, Neuroscience of affect: brain mechanisms of pleasure and displeasure. *Curr Opin Neurobiol* **23**, 294-303 (2013).

26.   J. R. Dalenberg, H. R. Hoogeveen, R. J. Renken, D. R. M. Langers, G. J. ter Horst, Functional specialization of the male insula during taste perception. *NeuroImage* **119**, 210-220 (2015).

27.   M. N. Baliki, P. Y. Geha, A. V. Apkarian, Parsing pain perception between nociceptive representation and magnitude estimation. *J Neurophysiol* **101**, 875-887 (2009).

28.   M. N. Baliki *et al.*, Parceling Human Accumbens into Putative Core and Shell Dissociates Encoding of Values for Reward and Pain. *Journal of Neuroscience* **33**, 16383-16393 (2013).

29.   G. Corder *et al.*, An amygdalar neural ensemble that encodes the unpleasantness of pain. *Science* **363**, 276-281 (2019).

30.   J. Kim, M. Pignatelli, S. Xu, S. Itohara, S. Tonegawa, Antagonistic negative and positive neurons of the basolateral amygdala. *Nature Neuroscience* **19**, 1636-1646 (2016).

31.   L. Wang *et al.*, The coding of valence and identity in the mammalian taste system. *Nature* **558**, 127-131 (2018).

32.   K. M. Tye, Neural Circuit Motifs in Valence Processing. *Neuron* **100**, 436-452 (2018).

33.   P. H. Janak, K. M. Tye, From circuits to behaviour in the amygdala. *Nature* **517**, 284-292 (2015).

34.   A. Nakao, Y. Takahashi, M. Nagase, R. Ikeda, F. Kato, Role of capsaicin-sensitive C-fiber afferents in neuropathic pain-induced synaptic potentiation in the nociceptive amygdala. *Mol Pain* **8**, 51 (2012).

35.   T. E. Kraynak, A. L. Marsland, T. D. Wager, P. J. Gianaros, Functional neuroanatomy of peripheral inflammatory physiology: A meta-analysis of human neuroimaging studies. *Neurosci Biobehav Rev* **94**, 76-92 (2018).

36.   I. Faillenot, R. A. Heckemann, M. Frot, A. Hammers, Macroanatomy and 3D probabilistic atlas of the human insula. *Neuroimage* **150**, 88-98 (2017).

37.   A. de la Vega, L. J. Chang, M. T. Banich, T. D. Wager, T. Yarkoni, Large-Scale Meta-Analysis of Human Medial Frontal Cortex Reveals Tripartite Functional Organization. *J Neurosci* **36**, 6553-6562 (2016).

38.   L. M. Bartoshuk *et al.*, Valid across-group comparisons with labeled scales: the gLMS versus magnitude matching. *Physiol Behav* **82**, 109-114 (2004).

39.   J. J. Lee *et al.*, A neuroimaging biomarker for sustained experimental and clinical pain. *Nat Med* **27**, 174-182 (2021).

40.   J. J. Lee, S. Lee, D. H. Lee, C. W. Woo, Functional brain reconfiguration during sustained pain. *Elife* **11** (2022).

41.   L. Fan *et al.*, The Human Brainnetome Atlas: A New Brain Atlas Based on Connectional Architecture. *Cerebral Cortex* **26**, 3508-3526 (2016).

42.   M. Roy *et al.*, Representation of aversive prediction errors in the human periaqueductal gray. *Nature Neuroscience* **17**, 1607-1612 (2014).

43.   F. Beissner, A. Schumann, F. Brunn, D. Eisenträger, K.-J. Bär, Advances in functional magnetic resonance imaging of the human brainstem. *NeuroImage* **86**, 91-98 (2014).

44.   B. T. Yeo *et al.*, The organization of the human cerebral cortex estimated by intrinsic functional connectivity. *J Neurophysiol* **106**, 1125-1165 (2011).

45.   L. E. Marks *et al.*, Magnitude-matching: the measurement of taste and smell. *Chemical Senses* **13**, 63-87 (1988).

46.   C.-W. Woo *et al.*, Quantifying cerebral contributions to pain beyond nociception. *Nature Communications* **8**, 14211 (2017).